SCIENCE CHINA
Information Sciences

• RESEARCH PAPER •

April 2025, Vol. 68, Iss. 4, 142201:1–142201:17
https://doi.org/10.1007/s11432-024-4293-3

Asymptotical event-based input-output constrained boundary control of flexible manipulator agents under a signed digraph

Xiangqian YAO[1], Xiangmin XU[1], Wei HE[2,3] & Yu LIU[4*]

[1]*School of Future Technology, South China University of Technology, Guangzhou 511442, China*
[2]*School of Automation and Institute of Artificial Intelligence, Beijing Information Science and Technology University, Beijing 102206, China*
[3]*School of Intelligence Science and Technology, University of Science and Technology Beijing, Beijing 100083, China*
[4]*School of Automation Science and Engineering, South China University of Technology, Guangzhou 510640, China*

Received 26 January 2024/Revised 29 October 2024/Accepted 8 January 2025/Published online 4 March 2025

Abstract This article tackles the boundary event-based bipartite consensus tracking control problem for the flexible manipulator multi-agent network over a signed diagraph. Each follower agent is the flexible manipulator with unknown disturbances, modeling uncertainties, input saturations and backlashes, and asymmetric output constraints. To reduce the continuous updating of control inputs, a new dynamic event-triggering mechanism is used. Under multiple constraints, achieving the asymptotic convergence point by point in space of the manipulator's vibration state is a control challenge. To solve this issue, we propose a new asymptotic convergence lemma. In control design, radial basis neural networks are employed to estimate nonlinear uncertain terms and the barrier Lyapunov function is used to accomplish the output constraints. Based on the Lyapunov direct method, a novel distributed boundary event-based control algorithm is designed to guarantee that the closed-loop network can reach the asymptotical bipartite consensus tracking and vibration suppression. Moreover, Zeno behaviors can be excluded for each agent. Finally, some numerical results are presented to demonstrate the validity and superiority of the designed control algorithm.

Keywords flexible-link manipulator, input-output constraint, event-based, asymptotical bipartite tracking, vibration control

Citation Yao X Q, Xu X M, He W, et al. Asymptotical event-based input-output constrained boundary control of flexible manipulator agents under a signed digraph. Sci China Inf Sci, 2025, 68(4): 142201, https://doi.org/10.1007/s11432-024-4293-3

1 Introduction

The consensus control of multi-agent systems (MASs) has garnered significant attention recently because of its extensive application in formation control, unmanned air vehicles and intelligent traffics [1–3]. Consensus tracking is a special consensus control where all agents collaborate to achieve the reference behavior determined by the leader agent [4]. Typically, all agents reach consensus through cooperative interactions between all nodes represented by an unsigned graph with non-negative edge weights. However, in many real-world situations, agents may interact in both cooperative and competitive ways, and a signed graph can be used to depict a communication network in which agents engage in both competitive and cooperative interactions [5–7]. Based on a directed signed graph, the bipartite tracking consensus problem for high-order heterogeneous nonlinear and uncertain MASs is addressed in [8]. Under communication time-varying delays, the authors deal with the bipartite tracking consensus problem for high-order nonlinear MASs in [9]. Nevertheless, the aforementioned research results are all derived from lumped parameter systems (LPSs) about time variable. Actually, state variables of numerous physical systems are typically linked not only to time, but also to space [10–12]. Flexible spacecraft, flexible manipulators, and axially moving belts are common examples of distributed parameter systems (DPSs) [13–16]. These studies focus on developing boundary control algorithms to suppress vibrations in a single flexible mechanical system, but they neglect the cooperative control of multiple flexible systems, in which the angle consensus tracking of multiple flexible manipulators and spacecraft are typical practical scenarios.

* Corresponding author (email: auylau@scut.edu.cn)

Compared to LPSs, DPSs present greater challenges for consensus tracking control due to their dynamic coupling. Some results have been proposed for boundary consensus tracking based on undirected or directed unsigned graphs [17–22]. In [23], the asymptotical bipartite angle consensus tracking problem for multiple flexible-link manipulators is solved. The consensus tracking control of several movable flexible manipulators is addressed in [24]. With actuator faults and input saturations, a boundary fault-tolerant control is developed to accomplish bounded consensus tracking of multiple flexible-link manipulators [25]. In [26], an adaptive NN-based boundary control is designed for a flexible-link manipulator network under an undirected graph. Note that these existing results do not take the output constraints into account. In solving this problem, the barrier Lyapunov function (BLF) offers an appealing idea: the boundedness of the BLF realizes the output constraint of a system. Based on various BLFs, numerous results of constrained control research have been found for LPSs [27–29]. In [30], the authors investigated the practical fixed-time consensus tracking problem for multiple Euler-Lagrange systems with output constraints. By using time-varying BLF, a fixed-time adaptive NN controller is proposed for unknown robot manipulators in [31]. For DPSs, the BLF design is distinct. To eliminate some cross terms from system dynamics, BLFs are often designed as $\phi^2(t)F(\cdot)$ in [32–34], where $\phi(t)$ is the auxiliary variable and $F(\cdot)$ is the common BLF. However, these findings may not theoretically address the case of $\phi(t) = 0$. When $\phi(t) = 0$, the boundedness of $F(\cdot)$ is not guaranteed, which is a huge theoretical challenge for output constraint control of DPSs. The first feasible solution is to introduce a damping coefficient into the DPS model. By designing a log-type BLF, the bounded angle tracking and vibration suppression for a flexible manipulator with the damping coefficient are studied in [35]. The second feasible solution is to make $\phi(t) = \lambda s(t) + \dot{s}(t), \lambda > 0$. When $\phi(t) = \lambda s(t) + \dot{s}(t) = 0$, $s(t) = \mathrm{e}^{-\lambda t}s(0)$. If $s(0)$ is restrained, $s(t)$ can also be restrained, which can overcome the theoretical challenge of the output constraints of DPSs.

It should be emphasized that the above-discussed results are driven by time-triggered control. Compared with time-triggered control, event-triggered control (ETC) allows a trade-off between reducing controller updates and preserving desired system performances, thereby compressing control costs and saving resources [36–38]. Dynamic ETCs emerge as a need to achieve more resource-efficient and flexible design. In [39], an adaptive boundary dynamic ETC strategy is proposed for an aerial refueling hose system. Based on the backstepping method, the boundary dynamic ETC issue for reaction-diffusion systems has been addressed in [40]. For a class of reaction-diffusion equations, an observer-based dynamic boundary ETC strategy is provided in [41]. The existing research achievements for event-based consensus tracking control are nearly exclusively based on LPSs. Using a dynamic ETC algorithm, the containment control problem of networked Euler-Lagrange systems is investigated in [42]. The bipartite event-triggered consensus tracking issue is solved for linear MASs in [43]. The dynamic event-triggered output formation-containment tracking problem for linear MASs is considered in [44]. These existing dynamic ETCs have not completely examined the controlled system's input-output restrictions. It has not been discovered to examine the boundary dynamic ETC of a single flexible manipulator, let alone the event-based bipartite consensus tracking of several flexible manipulators, when input saturations and backlashes, output constraints, and disturbances are all simultaneously considered. Besides, achieving the spatial point-by-point asymptotic convergence of states of DPSs with multiple constraints keeps a control challenge since most of the existing boundary control algorithms can only achieve the ultimately uniformly bounded (UUB) convergence of closed-loop systems.

After the above analysis, we aim to address the boundary event-based bipartite consensus tracking control issue for a flexible manipulator agent network under time-varying disturbances, modeling uncertainties, input saturations and backlashes, and output constraints. By integrating the local interaction protocol, input-output constraint control, and dynamic event-triggering mechanism in control design, the spatial point-by-point asymptotic vibration suppression and bipartite consensus tracking control can be achieved over a signed diagraph. In general, the major contribution has three aspects.

(1) Compared with the existing results in [21–25], the boundary bipartite consensus tracking of flexible manipulator agents can be further achieved on a signed graph, and the proposed consensus control algorithm can guarantee both transient and steady-state performances, despite the influence of input saturations and backlashes, uncertain modeling dynamics, and unknown disturbances.

(2) The adaptive neural network is used to estimate the sum of the saturation error term and the uncertain dynamic. By doing this, the proposed control algorithm can address the input backlash effect even if the slope of backlash is unknown, but Refs. [12, 15] cannot deal with this case. Besides, a new boundary dynamic event-based control strategy is proposed and is composed of a relative threshold, a non-negative $\mathcal{L}_1$-integrable function, and a new interval dynamic variable. Different from the dynamic

event-based mechanisms in [39, 42, 44], the proposed triggering conditions are more difficult to meet, resulting in some longer dwell times.

(3) Under a new inequality condition, we reveal an interesting asymptotic convergence result. It provides a solution to realize the spatial point-by-point asymptotic convergence of vibration states for flexible manipulator systems under multiple uncertain constraints. Hence, it can achieve steady-state performance that converges to zero, thereby further improving the control accuracy of UUB results in [12, 13, 15, 16, 20, 25, 26, 32–34].

The layout of this work is organized as follows. In Section 2, problem statements and some preliminaries are introduced. Boundary event-based consensus design and stability analysis are provided in Section 3. Simulation results are presented in Section 4. The conclusion is summarized in Section 5.

2 Problem statements and preliminaries

2.1 Signed diagraph

A diagraph is a pair $\mathcal{G} = \{\mathcal{V}_\mathcal{G}, \mathcal{E}_\mathcal{G}\}$, where $\mathcal{V}_\mathcal{G} = \{1, \ldots, N\}$ is the node set and $\mathcal{E}_\mathcal{G} \subset \mathcal{V}_\mathcal{G} \times \mathcal{V}_\mathcal{G}$ is edge set of ordered pairs of nodes. The edge (j, i) in the edge set of a diagraph denotes that node j can obtain information from node i, but not necessarily vice versa. Moreover, self-edges (i, i) are not allowed. A signed digraph $\mathcal{G}$ is a triple $\mathcal{G} = \{\mathcal{V}_\mathcal{G}, \mathcal{E}_\mathcal{G}, \mathcal{W}_\mathcal{G}\}$, where the node set $\mathcal{V}_\mathcal{G} = \{1, \ldots, N\}$, the edge set $\mathcal{E}_\mathcal{G} \subset \mathcal{V}_\mathcal{G} \times \mathcal{V}_\mathcal{G}$, and the adjacency matrix $\mathcal{W}_\mathcal{G} = [w_{ij}]_{N\times N}$ with $w_{ij} \neq 0 \Leftrightarrow (j, i) \in \mathcal{E}_\mathcal{G}$. $w_{ij} = 1$ ($w_{ij} = -1$) describes the cooperative interaction (antagonistic interaction) between agents. Let $\mathcal{N}_i = \{j : (j, i) \in \mathcal{E}_\mathcal{G}\}$ denote the neighbouring nodes of node i. Laplacian matrix of $\mathcal{G}$ is denoted by $\mathcal{L}_\mathcal{G} = [\mathcal{L}_{ij}]_{N\times N}$, in which $\mathcal{L}_{ij} = -w_{ij}$ for $i \neq j$ and $\mathcal{L}_{ii} = \sum_{j\in\mathcal{N}_i} |w_{ij}|$. Signed diagraph $\mathcal{G}$ containing the leader node 0 is the augmented diagraph $\bar{\mathcal{G}} = \{\bar{\mathcal{V}}_\mathcal{G}, \bar{\mathcal{E}}_\mathcal{G}\}$, where $\bar{\mathcal{V}}_\mathcal{G} = \mathcal{V}_\mathcal{G} \cup \{0\}$, $\bar{\mathcal{E}}_\mathcal{G} \subset \bar{\mathcal{V}}_\mathcal{G} \times \bar{\mathcal{V}}_\mathcal{G}$. $\mathcal{B}_0 = \mathrm{diag}\{b_1, \ldots, b_N\}$ is the pinning matrix, where $b_i = 1$ denotes node i can receive the directed information from leader 0; $b_i = 0$, otherwise. Then, the interaction matrix $\mathcal{H} = \mathcal{B}_0 + \mathcal{L}_\mathcal{G}$. Generally, node i is called to have a directed path to node k if there exists a distinct sequence of $i_1, \ldots, i_m$ such that $(i_1, i_2), \ldots, (i_{m-1}, i_m), (i_m, k) \in \bar{\mathcal{E}}_\mathcal{G}$. If there exists at least one directed path in $\bar{\mathcal{G}}$ from at least one node to all the other nodes, $\bar{\mathcal{G}}$ is called contains a directed spanning tree.

$\mathcal{G}$ is structurally balanced if: (1) there exists a bipartition of node sets $\mathcal{V}_{\mathcal{G}1}$ and $\mathcal{V}_{\mathcal{G}2}$ such that $\mathcal{V}_\mathcal{G} = \mathcal{V}_{\mathcal{G}1} \cup \mathcal{V}_{\mathcal{G}2}$, $\mathcal{V}_{\mathcal{G}1} \cap \mathcal{V}_{\mathcal{G}2} = \varnothing$ and $w_{ij} = 1$ if $(j, i) \in \mathcal{V}_{\mathcal{G}p} (p = 1, 2)$, and when $i \in \mathcal{V}_{\mathcal{G}p}, i \in \mathcal{V}_{\mathcal{G}(3-p)}, w_{ij} = -1$; (2) there exists a gauge transformation matrix $\mathcal{A} = \mathrm{diag}\{a_1, \ldots, a_N\}$ such that $a_i = 1$ if node $i \in \mathcal{V}_{\mathcal{G}1}$ and $a_i = -1$ if node $i \in \mathcal{V}_{\mathcal{G}2}$. Based on the gauge transformation matrix $\mathcal{A} = \mathrm{diag}\{a_1, \ldots, a_N\}$, $\mathcal{G}$ can be converted to an unsigned diagraph with the same structure [5]. Then, $\mathcal{G}$ is structurally balanced if and only if (iff) there exists a gauge transformation matrix $\mathcal{A}$ such that $\bar{\mathcal{W}}_\mathcal{G} = \mathcal{A}\mathcal{W}_\mathcal{G}\mathcal{A}$ is with all non-negative entries, and $\bar{\mathcal{L}}_\mathcal{G} = \mathcal{A}\mathcal{L}_\mathcal{G}\mathcal{A}$ has all non-positive off-diagonal entries [5]. Besides, if unsigned $\bar{\mathcal{G}}$ contains a directed spanning tree, there exists a $\mathcal{D} = \mathrm{diag}\{d_1, \ldots, d_N\}$ such that $\bar{\mathcal{H}} = \mathcal{H}^{\mathrm{T}}\mathcal{D} + \mathcal{D}\mathcal{H}$ is positive definite where $d = [d_1, \ldots, d_N]^{\mathrm{T}}$ is from $d = \mathcal{H}^{-\mathrm{T}}\mathbf{1}_N$ [4].

Assumption 1. $\bar{\mathcal{G}}$ contains a directed spanning tree rooted at node 0 and is structurally balanced.

Remark 1. By using the gauge transformation matrix $\mathcal{A}$, $\mathcal{L}_\mathcal{G}$ can be transformed into the new Laplacian matrix $\mathcal{A}\mathcal{L}_\mathcal{G}\mathcal{A}$ of the corresponding unsigned graph. And, $\mathcal{A}\mathcal{H}\mathcal{A} = \mathcal{B}_0 + \mathcal{A}\mathcal{L}_\mathcal{G}\mathcal{A}$ is an interaction matrix of the unsigned diagraph. Under Assumption 1, $\tilde{\mathcal{H}} = \mathcal{A}\bar{\mathcal{H}}\mathcal{A} = (\mathcal{A}\mathcal{H}\mathcal{A})^{\mathrm{T}}\mathcal{D} + \mathcal{D}\mathcal{A}\mathcal{H}\mathcal{A}$ is positive definite, where $d = \mathcal{A}\mathcal{H}^{-\mathrm{T}}\mathcal{A}\mathbf{1}_N$. Moreover, $\bar{\mathcal{H}}$ is also positive definite.

2.2 Problem statements

The considered follower agent is the flexible-link manipulator described in Figure 1, where it is composed of an Euler-Bernoulli beam, a rotatable rigid hub, and a tip payload. In coordinate systems SoY and soy, $y_i(s, t) \in \mathbb{R}$ and $\theta_i(t) \in \mathbb{R}$ characterize the vibration displacement and angle displacement of the manipulator. The total displacement of the manipulator is $x_i(s, t) = s\theta_i(t) + y_i(s, t), s \in [0, l_i]$. $l = l_i, \rho_i, E_iI_i, T_i, c_i$ respectively denote the length of the link, mass per unit length, bending stiffness, tension and damping coefficient. Moreover, the inertia of the hub is I_{hi}, and the mass of the tip payload is m_i. $u_{mi}(t)$ is the control input force and $d_{mi}(t)$ is the disturbance, where $m = 1, 2$. It is assumed that there exist some unknown positive constants $\bar{d}_{mi}, m = 1, 2$, such that $|d_{mi}| \leqslant \bar{d}_{mi}$ [35].

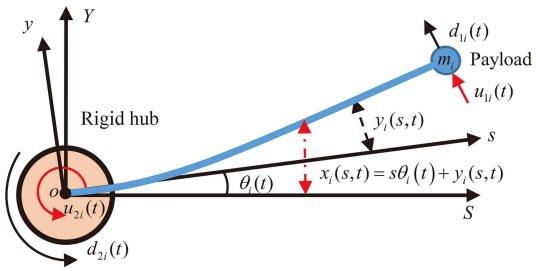

Figure 1 (Color online) Schematic diagram of the i-th flexible manipulator.

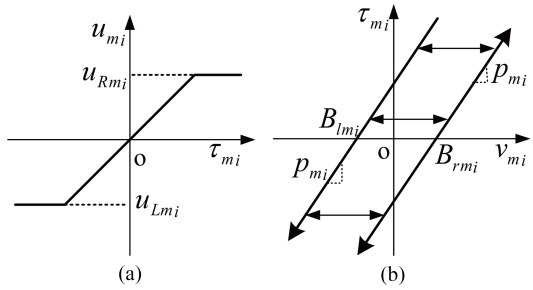

Figure 2 Input constraints. (a) Saturation; (b) backlash.

Remark 2. In the sequel, we set $(*)(s,t)=(*)(s)$ and $(*)(t)=(*)$, $\forall s\in[0,l]$, $t\in[0,\infty)$. Moreover, let $(*)'=\frac{\partial(*)}{\partial s}$, $(*)''=\frac{\partial^2(*)}{\partial^2 s}$, $(*)'''=\frac{\partial^3(*)}{\partial^3 s}$,$(*)''''=\frac{\partial^4(*)}{\partial^4 s}$, $(\dot{*})=\frac{\partial(*)}{\partial t}$, $(\ddot{*})=\frac{\partial^2(*)}{\partial^2 t}$.

Consider a signed multi-agent network with one leader and N followers. In network, the i-th flexible manipulator follower agent is modeled as [35]

$$\rho_i\ddot{x}_i(s)+E_iI_iy_i''''(s)-T_iy_i''(s)+c_i\dot{x}_i(s)=0, \tag{1a}$$

$$y_i(0)=y_i'(0)=y_i''(l_i)=0, \tag{1b}$$

$$m_i\ddot{x}_i(l_i)-E_iI_iy_i'''(l_i)+T_iy_i'(l_i)-f_{1i}-u_{1i}-d_{1i}=0, \tag{1c}$$

$$I_{hi}\ddot{\theta}_i-T_iy_i(l_i)-E_iI_iy_i''(0)-f_{2i}-u_{2i}-d_{2i}=0, \tag{1d}$$

where $i\in\{1,\dots,N\}$, and $f_{mi}=f_{mi}(\mathcal{X}_{mi})$, $m=1,2$, are the continuous modeling uncertainties with $\mathcal{X}_{1i}=[\dot{x}_i(l_i),x_i(l_i),y_i'(l_i),y_i'''(l_i)]^{\mathrm{T}}$, and $\mathcal{X}_{2i}=[\dot{\theta}_i,\theta_i,y_i(l_i),y_i''(0)]^{\mathrm{T}}$.

Input saturation described in Figure 2(a) is a common actuator issue and is denoted by

$$u_{mi}=\mathrm{Sat}(\tau_{mi})=\begin{cases}u_{Rmi}, & \text{if } \tau_{mi}\geqslant u_{Rmi},\\ \tau_{mi}, & \text{if } u_{Lmi}<\tau_{mi}<u_{Rmi},\\ u_{Lmi}, & \text{if } \tau_{mi}\leqslant u_{Lmi},\end{cases} \tag{2}$$

where τ_{mi} is the control input, $u_{Lmi}<0$ and $u_{Rmi}>0$ are the saturation boundary constants of u_{mi}.

Besides, input backlash described in Figure 2(b) also exists widely in systems and is modeled as

$$\tau_{mi}=\begin{cases}p_{mi}(v_{mi}-B_{rmi}), & \text{if } \dot{v}_{mi}>0 \text{ and } \tau_{mi}=p_{mi}(v_{mi}-B_{rmi}),\\ p_{mi}(v_{mi}-B_{lmi}), & \text{if } \dot{v}_{mi}<0 \text{ and } \tau_{mi}=p_{mi}(v_{mi}-B_{lmi}),\\ \tau_{mi}(t_-), & \text{otherwise},\end{cases} \tag{3}$$

where $m=1,2$, $p_{mi}>0$ is the unknown slope of the line, $B_{rmi}>0$ and $B_{lmi}<0$ are the unknown constants, and $\tau_{mi}(t_-)$ denotes the backlash output τ_{mi} keep unchange when $\dot{v}_{mi}=0$.

Based on (3), we can formulate the input backlash τ_{mi} as

$$\tau_{mi}=\eta_{ri}p_{mi}(v_{mi}-B_{rmi})+\eta_{li}p_{mi}(v_{mi}-B_{lmi})+\eta_{si}\tau_{smi}, \tag{4}$$

where τ_{smi} is a generic constant and it satisfies $p_{mi}(v_{mi}-B_{rmi})\leqslant\tau_{smi}\leqslant p_{mi}(v_{mi}-B_{lmi})$, and $\eta_{ri}=1$ if $\dot{v}_{mi}>0$, $\eta_{ri}=0$, otherwise; $\eta_{li}=1$ if $\dot{v}_{mi}<0$, $\eta_{li}=0$, otherwise; $\eta_{si}=1$ if $\dot{v}_{mi}=0$, $\eta_{si}=0$, otherwise. Anyway, it always has $\eta_{ri}+\eta_{li}+\eta_{si}=1$.

Consider that $\theta_0=\theta_d$ and $y_0(l_0)=0$ as the leader, where θ_d is the desired constant tracking angle.

Definition 1. The network described by (1a)–(1d) achieves the asymptotical bipartite consensus tracking if there holds

$$\lim_{t\to\infty}|\theta_i-a_i\theta_0|=0,\ \lim_{t\to\infty}|l_i(\theta_i-a_i\theta_0)+y_i(l_i)|=0,\ i\in\mathcal{V}_{\mathcal{G}}, \tag{5}$$

where $a_i=1$ or $a_i=-1$.

Define the tracking errors as

$$\alpha_{1i}=l_i\alpha_{2i}+y_i(l_i),\quad \alpha_{2i}=\theta_i-a_i\theta_0. \tag{6}$$

To realize bipartite consensus tracking, the following local interaction protocol is designed as

$$\beta_m = (\mathcal{H}^{\mathrm{T}}\mathcal{D} + \mathcal{D}\mathcal{H})\alpha_m = \bar{\mathcal{H}}\alpha_m, \quad m = 1, 2, \tag{7}$$

where $\bar{\mathcal{H}}$ is positive definite according to Remark 1, $\alpha_m = [\alpha_{m1}, \ldots, \alpha_{mN}]^{\mathrm{T}}$, $\beta_m = [\beta_{m1}, \ldots, \beta_{mN}]^{\mathrm{T}}$.

To constrain the transient performances, α_{1i} and α_{2i} are required to meet the output constraints as

$$\Omega_{mi} = \left\{\beta_{mi} \in \mathbb{R} \middle| -\underline{h}_{mi} < \beta_{mi} < \bar{h}_{mi}\right\}, \quad t \geqslant 0, \tag{8}$$

where $\bar{h}_{mi}$, $\underline{h}_{mi}$, $m = 1, 2$, are some known positive constants. It is worth mentioning that when constraint control (8) is satisfied, we have $-\underline{h}_m < \beta_m = \bar{\mathcal{H}}\alpha_m < \bar{h}_m$. Furthermore, $-\bar{\mathcal{H}}^{-1}\underline{h}_m < \alpha_m < \bar{\mathcal{H}}^{-1}\bar{h}_m$.

Under multiple constraints, including input saturations and backlashes, unknown disturbances, and modeling uncertainties, control objectives in this work are to develop a novel distributed event-based boundary control algorithm to achieve:

(1) The asymptotical vibration suppression: $\lim_{t\to\infty} y_i(s) = 0$, $\forall s \in [0, l]$, and the asymptotical bipartite consensus tracking (5), where $i = 1, \ldots, N$;

(2) The performance constrain control (8) and to avoid Zeno behaviors for each agent.

2.3 Useful lemmas

Lemma 1. Suppose $\eta_1(s)$, $\eta_2(s) \in \mathbb{R}$, $s \in [0, l]$, it holds

$$\eta_1(s)\eta_2(s) \leqslant |\eta_1(s)||\eta_2(s)| \leqslant \frac{\varsigma}{2}\eta_1^2(s) + \frac{1}{2\varsigma}\eta_2^2(s), \ \varsigma > 0. \tag{9}$$

Lemma 2 ([35])**.** If $\eta(s), \eta'(s), \eta''(s) \in \mathcal{L}_2(0, l)$ and $\eta(0) = 0$, $\eta'(0) = 0$, the following equalities are:

$$\eta^2(s) \leqslant l\int_0^l [\eta'(s)]^2 \mathrm{d}s, \quad (\eta'(s))^2 \leqslant l\int_0^l [\eta''(s)]^2 \mathrm{d}s. \tag{10}$$

Lemma 3 ([20])**.** For any continuous function $f(\mathcal{X})$ defined on a compact set $\mathcal{X} \in \Omega \subset \mathbb{R}^n$, a radial basis function neural network (RBFNN) can be adopted to approximate a function $f(\mathcal{X})$ as

$$f(\mathcal{X}) = \mathcal{W}^{*\mathrm{T}}\Phi(\mathcal{X}) + \varepsilon(\mathcal{X}), \tag{11}$$

where $|\varepsilon(\mathcal{X})| \leqslant \varepsilon$, $\varepsilon > 0$, $\mathcal{W}^*$ is the ideal weight matrix described as $\mathcal{W}^* = \arg\min_{\mathcal{W}\in\mathbb{R}^n}\{\sup_{\mathcal{X}\in\Omega}|f(\mathcal{X}) - \mathcal{W}^{\mathrm{T}}\Phi(\mathcal{X})|\}$. Moreover, $\mathcal{X} = [\mathcal{X}_1, \ldots, \mathcal{X}_q]^{\mathrm{T}} \in \mathbb{R}^q$ is the input vector, $\Phi(\mathcal{X}) = [\Phi_1(\mathcal{X}), \ldots, \Phi_p(\mathcal{X})]^{\mathrm{T}} \in \mathbb{R}^p$ is the basis function vector and $\Phi_i(\mathcal{X})$ is chosen a Gaussian function as

$$\Phi_i(\mathcal{X}) = \mathrm{e}^{-(\mathcal{X}-C_i)^{\mathrm{T}}(\mathcal{X}-C_i)/B_i^2}, \ i = 1, \ldots, p, \tag{12}$$

where B_i is the width of the Gaussian function and $C_i \in \mathbb{R}^q$ is the center of the receptive field.

Lemma 4. Let $\mathcal{V}_a$ and $\mathcal{V}_b$ be two continuously differentiable positive definite functions on $[0, \infty)$, and $\dot{\mathcal{V}}_b$ is uniformly bounded on $[0, \infty)$. Suppose $q \in \mathcal{L}_1(0, \infty)$ is a non-negative real-valued function. If the following inequality is satisfied as:

$$\dot{\mathcal{V}}_a \leqslant -\iota\mathcal{V}_b + q, \ \mathcal{V}_b \leqslant \mathcal{V}_a, \tag{13}$$

then $\lim_{t\to\infty}\mathcal{V}_b = 0$ when $\mathcal{V}_a(0)$ is bounded. Specially, when $\mathcal{V}_c = \mathcal{V}_a - \mathcal{V}_b$ is a monotonic function, the uniformly bounded requirement for $\dot{\mathcal{V}}_b$ can be removed.

Proof. Letting $\mathcal{V}_c = \mathcal{V}_a - \mathcal{V}_b$, it is non-negative. When $\mathcal{V}_c$ is not monotonic, it follows from (13) that

$$\iota\int_0^t \mathcal{V}_b(\tau)\mathrm{d}\tau + \mathcal{V}_a \leqslant \mathcal{V}_a(0) + \int_0^t q(\tau)\mathrm{d}\tau < \infty, \tag{14}$$

which implies that $\mathcal{V}_b \in \mathcal{L}_1(0, \infty) \cap \mathcal{L}_\infty(0, \infty)$. Since $\dot{\mathcal{V}}_b \in \mathcal{L}_\infty(0, \infty)$ and using the Barbalat's lemma in [45], one has $\lim_{t\to\infty}\mathcal{V}_b = 0$.

When $\mathcal{V}_c$ is monotonic, by multiplying $\mathrm{e}^{\iota t}$ on both sides of (13), we obtain

$$\mathcal{V}_b \leqslant \mathrm{e}^{-\iota t}\mathcal{V}_b(0) + \mathrm{e}^{-\iota t}\int_0^t \mathrm{e}^{\iota\tau}(q(\tau) - \dot{\mathcal{V}}_c(\tau))\mathrm{d}\tau. \tag{15}$$

Due to $\int_0^t \mathrm{e}^{\iota\tau}\dot{\mathcal{V}}_c(\tau)\mathrm{d}\tau = \mathrm{e}^{\iota t}\mathcal{V}_c - \mathcal{V}_c(0) - \iota\int_0^t \mathrm{e}^{\iota\tau}\mathcal{V}_c(\tau)\mathrm{d}\tau$, it can further follow from (15) that

$$\mathcal{V}_b \leqslant \mathrm{e}^{-\iota t}(\mathcal{V}_b(0) + \mathcal{V}_c(0)) - \mathcal{V}_c + \int_0^t \mathrm{e}^{-\iota(t-\tau)}(q(\tau) + \iota\mathcal{V}_c(\tau))\mathrm{d}\tau. \tag{16}$$

Next, we will prove that for any $\delta > 0$ there always exits a $t_0 > 0$ such that $\mathcal{V}_b < \delta$ holds for any $t \geqslant t_0$.

Due to $q \in \mathcal{L}_1(0,\infty)$, it implies there exists a $t_1 > 0$ such that $\int_{t_1}^t q(\tau)\mathrm{d}\tau < \delta_1$ for any $\delta_1 > 0$. By decomposing the integral interval at t_1 for (16), one can yield

$$\mathcal{V}_b < \delta_1 + \mathrm{e}^{-\iota(t-t_1)}\int_0^{t_1} \mathrm{e}^{-\iota(t_1-\tau)}q(\tau)\mathrm{d}\tau + \mathrm{e}^{-\iota t}(\mathcal{V}_b(0) + \mathcal{V}_c(0)) + \iota\int_0^t \mathrm{e}^{-\iota(t-\tau)}\mathcal{V}_c(\tau)\mathrm{d}\tau - \mathcal{V}_c. \tag{17}$$

Moreover, it further derives

$$\mathcal{V}_b < \Big[\mathcal{V}_b(0) + \mathcal{V}_c(0) + \mathrm{e}^{\iota t_1}\|q\|_{\mathcal{L}_1(0,\infty)}\Big]\mathrm{e}^{-\iota t} + \delta_1 + \iota\int_0^t \mathrm{e}^{-\iota(t-\tau)}\mathcal{V}_c(\tau)\mathrm{d}\tau - \mathcal{V}_c. \tag{18}$$

Note that $\mathcal{V}_c \leqslant \mathcal{V}_a \in \mathcal{L}_\infty(0,\infty)$ and it is monotonic, we can know $\lim_{t\to\infty}\mathcal{V}_c$ exists. By using the L'Hospital principle, we can observe that

$$\lim_{t\to\infty}\iota\int_0^t \mathrm{e}^{-\iota(t-\tau)}\mathcal{V}_c(\tau)\mathrm{d}\tau = \lim_{t\to\infty}\frac{l\mathrm{e}^{lt}\mathcal{V}_c}{l\mathrm{e}^{lt}} = \lim_{t\to\infty}\mathcal{V}_c. \tag{19}$$

From (19), $\lim_{t\to\infty}\iota\int_0^t \mathrm{e}^{-\iota(t-\tau)}\mathcal{V}_c(\tau)\mathrm{d}\tau = \lim_{t\to\infty}\mathcal{V}_c$ and thereby $\lim_{t\to\infty}(\iota\int_0^t \mathrm{e}^{-\iota(t-\tau)}\mathcal{V}_c(\tau)\mathrm{d}\tau - \mathcal{V}_c) = 0$. Then, there exists a $t_2 > 0$ such that $|\iota\int_0^t \mathrm{e}^{-\iota(t-\tau)}\mathcal{V}_c(\tau)\mathrm{d}\tau - \mathcal{V}_c| < \delta_2$ for any $t \geqslant t_2$ and any $\delta_2 > 0$.

Letting $M_0 = \mathcal{V}_b(0) + \mathcal{V}_c(0) + \mathrm{e}^{\iota t_1}\|q\|_{\mathcal{L}_1(0,\infty)}$ and $\delta_1 = \frac{\delta}{3}, \delta_2 = \frac{\delta}{3}$ and taking $t_0 = \max\{t_1, t_2, \frac{1}{\iota}\ln\frac{3M_0}{\delta}\}$. Then for any $t \geqslant t_0$, we can always obtain

$$\mathcal{V}_b < \frac{\delta}{3} + \frac{\delta}{3} + \frac{\delta}{3} = \delta, \tag{20}$$

which implies that $\lim_{t\to\infty}\mathcal{V}_b = 0$.

Remark 3. This lemma provides an alternative solution to achieve asymptotic convergence of some adaptive systems. In particular, when $\mathcal{V}_c = \mathcal{V}_a - \mathcal{V}_b$ is a monotonic function ($\mathcal{V}_a = \mathcal{V}_b$ as a special case), Lemma 4 can remove the bounded requirement of the time derivative of the Lyapunov function in Barbalat's lemma, which has potential applications in adaptive distributed observer design. When $q = 0$, this proposed lemma will degrade into the differential inequality: $\dot{\mathcal{V}} \leqslant -f$ in [11]. Hence, our proposed lemma is an improved result. In Lemma 4, only $-\iota\mathcal{V}_b$ rather than $-\iota\mathcal{V}_a$ need to be given on the right-hand side of the inequality, which is more common in adaptive systems. However, one needs to check $\dot{\mathcal{V}}_b$ is uniformly bounded on $[0,\infty)$.

3 Control design and stability analysis

In this section, boundary consensus control, dynamic ETC, and BLF are integrated to design the corresponding control algorithm.

3.1 Boundary control algorithm design

Based on (4), we can rewrite the backlash effect (3) as

$$\tau_{mi} = p_{mi}v_{mi} + b_{mi}, \tag{21}$$

where b_{mi} is the remaining term and satisfies that $b_{mi} = -p_{mi}B_{rmi}$ if $\dot{v}_{mi} > 0$; $b_{mi} = -p_{mi}B_{lmi}$ if $\dot{v}_{mi} < 0$; $b_{mi} = \tau_{smi} - p_{mi}v_{mi}$ when $\dot{v}_{mi} = 0$. Moreover, it leads to $|b_{mi}| \leqslant \max\{p_{mi}|B_{rmi}|, p_{mi}|B_{lmi}|\}$.

Then, the boundary control input u_{mi} can be taken as

$$u_{mi} = v_{mi} + \mathrm{Sat}(p_{mi}v_{mi} + b_{mi}) - v_{mi} = v_{mi} - \Delta(v_{mi}), \tag{22}$$

where v_{mi} is the designed control input and $\Delta(v_{mi}) = \mathrm{Sat}(p_{mi}v_{mi} + b_{mi}) - v_{mi}$ is the saturation error.

Letting $g_{mi}(\bar{\mathcal{X}}_{mi}) = f_{mi}(\mathcal{X}_{mi}) + \Delta(v_{mi})$, then we can use Lemma 3 to estimate it as

$$g_{mi}(\bar{\mathcal{X}}_{mi}) = \mathcal{W}_{mi}^{*\mathrm{T}}\Phi_{mi}(\bar{\mathcal{X}}_{mi}) + \varepsilon_{mi}(\bar{\mathcal{X}}_{mi}), \tag{23}$$

where $\bar{\mathcal{X}}_{mi} = [\mathcal{X}_{mi}^{\mathrm{T}}, v_{mi}]^{\mathrm{T}}$ is the input variable of network.

From (22) and (23), the compact vector forms of boundary dynamics (1c) and (1d) can be rewritten as follows:

$$M\ddot{x}(l) = \Gamma_1 + v_1 + \mathcal{W}_1^{*\mathrm{T}}\Phi_1(\bar{\mathcal{X}}_1) + \mathcal{D}_1, \tag{24}$$

$$I_h\ddot{\theta} = \Gamma_2 + v_2 + \mathcal{W}_2^{*\mathrm{T}}\Phi_2(\bar{\mathcal{X}}_2) + \mathcal{D}_2, \tag{25}$$

where $M = \mathrm{diag}\{m_1, \ldots, m_N\}$, $I_h = \mathrm{diag}\{I_{h1}, \ldots, I_{hN}\}$, and $\ddot{x}(l) = [\ddot{x}_1(l), \ldots, \ddot{x}_N(l)]^{\mathrm{T}}$, $\ddot{\theta} = [\ddot{\theta}_1, \ldots, \ddot{\theta}_N]^{\mathrm{T}}$, $v_m = [v_{m1}, \ldots, v_{mN}]^{\mathrm{T}}$, $\Gamma_m = [\Gamma_{m1}, \ldots, \Gamma_{mN}]^{\mathrm{T}}$ with $\Gamma_{1i} = E_iI_iy_i'''(l) - T_iy_i'(l)$, $\Gamma_{2i} = T_iy_i(l) + E_iI_iy_i''(0)$, $\mathcal{W}_m^{*\mathrm{T}} = \mathrm{diag}\{\mathcal{W}_{m1}^{*\mathrm{T}}, \ldots, \mathcal{W}_{mN}^{*\mathrm{T}}\}$, and $\Phi_m(\bar{\mathcal{X}}_m) = [\Phi_{m1}(\bar{\mathcal{X}}_{m1}), \ldots, \Phi_{mN}(\bar{\mathcal{X}}_{mN})]^{\mathrm{T}}$, $\mathcal{D}_m = [\mathcal{D}_{m1}, \ldots, \mathcal{D}_{mN}]^{\mathrm{T}}$, where $\mathcal{D}_{mi} = d_{mi} + \varepsilon_{mi}(\bar{\mathcal{X}}_{mi})$ and $|\mathcal{D}_{mi}| \leqslant \bar{\mathcal{D}}_{mi} = \bar{d}_{mi} + \bar{\varepsilon}_{mi}, m = 1, 2$.

To achieve the control objectives, the actual compact control inputs can be designed as

$$\begin{aligned} v_m = {} & -k_m\dot{\beta}_m - \kappa_m s_m - \bar{\kappa}_m\beta_m - \left((1 - q(\beta_m))\sec^2\left(\frac{\pi\beta_m^2}{2\underline{h}_m^2}\right)\right. \\ & \left. + q(\beta_m)\sec^2\left(\frac{\pi\beta_m^2}{2\bar{h}_m^2}\right)\right)\nu^{-1}\bar{\mathcal{H}}\beta_m - \hat{\mathcal{W}}_m^{\mathrm{T}}\Phi_m(\bar{\mathcal{X}}_m) - \frac{s_m\hat{\mathcal{D}}_m}{|s_m| + \varphi_m}, \end{aligned} \tag{26}$$

$$\dot{\hat{\mathcal{W}}}_{mi} = \sigma_{mi}s_{mi}\Phi_{mi}(\mathcal{X}_{mi}) - \sigma_{mi}\varrho_{mi}\hat{\mathcal{W}}_{mi}, \tag{27}$$

$$\dot{\hat{\mathcal{D}}}_{mi} = \frac{\varpi_{mi}s_{mi}^2}{|s_{mi}| + \varphi_{mi}} - \varpi_{mi}\varrho_{mi}\hat{\mathcal{D}}_{mi}, \tag{28}$$

where $s_{1i} = \mu_i\beta_{1i} + \nu_i\dot{x}_i(l_i), s_{2i} = \mu_i\beta_{2i} + \nu_i\dot{\theta}_i$, $k_m = \mathrm{diag}\{k_{m1}, \ldots, k_{mN}\}$, $\kappa_m = \mathrm{diag}\{\kappa_{m1}, \ldots, \kappa_{mN}\}$, $\bar{\kappa}_m = \mathrm{diag}\{\bar{\kappa}_{m1}, \ldots, \bar{\kappa}_{mN}\}$, and $\nu = \mathrm{diag}\{\nu_1, \ldots, \nu_N\}$, $\mu = \mathrm{diag}\{\mu_1, \ldots, \mu_N\}$, are some diagonal positive definite matrices, and $(1-q(\beta_m))\sec^2(\frac{\pi\beta_m^2}{2\underline{h}_m^2}) = \mathrm{diag}\{(1-q(\beta_{m1}))\sec^2(\frac{\pi\beta_{m1}^2}{2\underline{h}_{m1}^2}), \ldots, (1-q(\beta_{mN}))\sec^2(\frac{\pi\beta_{mN}^2}{2\underline{h}_{mN}^2})\}$, $(1-q(\beta_m))\sec^2(\frac{\pi\beta_m^2}{2\underline{h}_m^2}) = \mathrm{diag}\{q(\beta_{m1})\sec^2(\frac{\pi\beta_{m1}^2}{2\underline{h}_{m1}^2}), \ldots, q(\beta_{mN})\sec^2(\frac{\pi\beta_{mN}^2}{2\underline{h}_{mN}^2})\}$, $\frac{s_m}{|s_m|+\varphi_m} = \mathrm{diag}\{\frac{s_{m1}}{|s_{m1}|+\varphi_{m1}}, \ldots, \frac{s_{mN}}{|s_{mN}|+\varphi_{mN}}\}$, and function $q(*)$ is defined as $q(*) = 1$ if $* > 0$ and $q(*) = 0$ when $* \leqslant 0$. Moreover, ϖ_{mi}, σ_{mi} are some positive constants, and $0 \leqslant \varphi_{mi} \in \mathcal{L}_1(0, \infty)$ and $0 \leqslant \varrho_{mi} \in \mathcal{L}_1(0, \infty)$, such as $\varrho_{mi} = \zeta_{mi}\mathrm{e}^{-\omega_{mi}t}$, where ζ_{mi}, ω_{mi} are some positive constants.

In order to save control resources, we further use the dynamic event-triggered mechanism:

$$\vartheta_{mi}(t) = v_{mi}(t_{mh}^i), \ \forall t \in [t_{mh}^i, t_{m(h+1)}^i), \ h \in \mathbb{Z}^+, \tag{29}$$

$$t_{m(h+1)}^i = \inf\{t > t_{mh}^i | f_{mi}(e_{mi}, \vartheta_{mi}, t) \geqslant 0\}, \tag{30}$$

$$f_{mi}(e_{mi}, \vartheta_{mi}, t) = e_{mi}^2 - \gamma_{mi}s_{mi}^2 - g_{mi} - \bar{\varphi}_{mi}, \tag{31}$$

$$\dot{g}_{mi} = \bar{\delta}_{mi}(\gamma_{mi}s_{mi}^2 - e_{mi}^2 + \bar{\varphi}_{mi}), \tag{32}$$

where $t_{m1}^i = 0$ and g_{mi} is the interval internal variable with $g_{mi}(0) > 0$ and $0 \leqslant \bar{\varphi}_{mi} \in \mathcal{L}_1(0, \infty)$, such as $\bar{\varphi}_{mi} = \mu_{mi}\mathrm{e}^{-\iota_{mi}t}$. And, γ_{mi}, $\bar{\delta}_{mi}$, μ_{mi}, ι_{mi} are some positive constants. Moreover, v_{mi} is the designed continuous controller and $e_{mi} = \vartheta_{mi} - v_{mi}$ is the measurement error, $m = 1, 2$.

Note that based on (30) and (31), we have $e_{mi}^2 - \gamma_{mi}s_{mi}^2 - \bar{\varphi}_{mi} \leqslant g_{mi}$. Then, it can follow from (32) that $\dot{g}_{mi} \geqslant -\bar{\delta}_{mi}g_{mi}$. It implies that $g_{mi} \geqslant g_{mi}(0)\mathrm{e}^{-\bar{\delta}_{mi}t} \geqslant 0$.

By plugging in the above event-triggered mechanism, it yields

$$m_i\ddot{x}_i(l_i) = \Gamma_{1i} + v_{1i} + e_{1i} + \mathcal{W}_{1i}^{*\mathrm{T}}\Phi_{1i}(\bar{\mathcal{X}}_{1i}) + \mathcal{D}_{1i}, \tag{33}$$

$$I_h\ddot{\theta}_i = \Gamma_{2i} + v_{2i} + e_{2i} + \mathcal{W}_{2i}^{*\mathrm{T}}\Phi_{2i}(\bar{\mathcal{X}}_{2i}) + \mathcal{D}_{2i}. \tag{34}$$

3.2 Lyapunov function design

Let $x_e(s) = s\beta_2 + \bar{\mathcal{H}}y(s) = \bar{\mathcal{H}}\alpha$ be a compact vector, where $x_e(s) = [x_{e1}(s), \ldots, x_{eN}(s)]^{\mathrm{T}}$. Firstly, choose the Lyapunov function candidate as

$$\mathcal{V}_0 = \mathcal{V}_1 + \mathcal{V}_2 + \mathcal{V}_3, \tag{35}$$

where $\mathcal{V}_1, \mathcal{V}_2, \mathcal{V}_3$, are separately defined as

$$\mathcal{V}_1 = \frac{1}{2}\sum_{i=1}^{N}\int_0^{l_i}\nu_i\rho_i\dot{x}^2(s) + \frac{1}{2}\sum_{i=1}^{N}\int_0^{l_i}\nu_i T_i(y_i'(s))^2\mathrm{d}s + \frac{1}{2}\sum_{i=1}^{N}\int_0^{l_i}\nu_i E_i I_i(y_i''(s))^2\mathrm{d}s, \tag{36}$$

$$\mathcal{V}_2 = \sum_{i=1}^{N}\mu_i m_i\beta_{1i}\dot{x}_i(l_i) + \sum_{i=1}^{N}\mu_i I_{hi}\beta_{2i}\dot{\theta}_i + \sum_{i=1}^{N}\int_0^{l_i}\mu_i\rho_i\dot{x}_i(s)x_{ei}(s)\mathrm{d}s, \tag{37}$$

$$\begin{aligned}\mathcal{V}_3 =& \frac{1}{2}\sum_{i=1}^{N}\mu_i k_{1i}\beta_{1i}^2 + \frac{1}{2}\sum_{i=1}^{N}\nu_i m_i\dot{x}_i^2(l_i) + \frac{1}{2}\sum_{i=1}^{N}\nu_i I_{hi}\dot{\theta}_i^2\\ &+ \frac{1}{2}\sum_{i=1}^{N}\mu_i k_{2i}\beta_{2i}^2 + \frac{1}{2}\sum_{m=1}^{2}\beta_m^{\mathrm{T}}\bar{\kappa}_m\nu\bar{\mathcal{H}}^{-1}\beta_m + \frac{1}{2}\int_0^{l}x_e^{\mathrm{T}}(s)c\mu\bar{\mathcal{H}}^{-1}x_e(s)\mathrm{d}s,\end{aligned} \tag{38}$$

where $\nu_i,\ \mu_i,\ k_{1i},\ k_{2i}$ are some positive constants.

Notice that $\mathcal{V}_2$ may be negative and thereby $\mathcal{V}_0$ cannot become a Lyapunov function. To ensure $\mathcal{V}_0$ is non-negative, we apply the Lemma 2 to estimate $|\mathcal{V}_2|$ as

$$\begin{aligned}|\mathcal{V}_2| \leqslant& \sum_{i=1}^{N}\left\{\int_0^{l}\left(\frac{\varsigma_1\rho_i\mu_i}{2}x_{ei}^2(s) + \frac{\mu_i\rho_i}{2\varsigma_1}\dot{x}_i^2(s)\right)\mathrm{d}s\right.\\ &\left.+ \frac{I_{hi}\mu_i}{2\varsigma_2}\dot{\theta}_i^2 + \frac{I_{hi}\mu_i\varsigma_2}{2}\beta_{1i}^2 + \frac{m_i\mu_i\varsigma_3}{2}\beta_{2i}^2 + \frac{m_i\mu_i}{2\varsigma_3}\dot{x}_i^2(l_i)\right\} \leqslant \Xi(\mathcal{V}_1 + \mathcal{V}_3),\end{aligned} \tag{39}$$

where $\Xi = \max\{\lambda_M(\varsigma_1 c^{-1}\rho\bar{\mathcal{H}}), \lambda_M(\varsigma_1^{-1}\mu\nu^{-1}), \lambda_M(\varsigma_2 M K_1^{-1}), \lambda_M(\varsigma_2^{-1}\mu\nu^{-1}), \lambda_M(\varsigma_3 I_h K_2^{-1}), \lambda_M(\varsigma_3^{-1}\mu\nu^{-1})\}$, and $\lambda_M(\star)$ denotes the maximum eigenvalue of matrix $\star$. If one takes $\mu,\ \nu,\ \varsigma_1,\ \varsigma_2,\ \varsigma_3,\ K_1,\ K_2$ such that $0 < \Xi < 1$ and use (39), one can yield

$$0 \leqslant (1-\Xi)(\mathcal{V}_1 + \mathcal{V}_3) \leqslant \mathcal{V}_0 \leqslant (1+\Xi)(\mathcal{V}_1 + \mathcal{V}_3), \tag{40}$$

which ensures the Lyapunov candidate $\mathcal{V}_0$ is non-negative.

Next, by substituting (1a)–(1c) and using the integration by part, we differentiate $\mathcal{V}_1$ with respect to time and can obtain

$$\begin{aligned}\dot{\mathcal{V}}_1 =& \sum_{i=1}^{N}\int_0^{l_i}\nu_i\dot{x}_i(s)\rho_i\ddot{x}_i(s) + \sum_{i=1}^{N}\int_0^{l_i}\nu_i T_i y_i'(s)\dot{y}_i'(s)\mathrm{d}s + \sum_{i=1}^{N}\int_0^{l_i}\nu_i E_i I_i y_i''(s)\dot{y}_i''(s)\mathrm{d}s\\ =& -\sum_{i=1}^{N}\nu_i\dot{x}_i(l_i)\Gamma_{1i} - \sum_{i=1}^{N}\nu_i\dot{\theta}_i\Gamma_{2i} - \sum_{i=1}^{N}\int_0^{l_i}\nu_i c_i\dot{x}_i^2(s)\mathrm{d}s.\end{aligned} \tag{41}$$

Similarly, by substituting (1a)–(1c) and applying the integration by part and using (6), (7), (33), and (34), then the time derivative of $\mathcal{V}_2$ can be obtained as

$$\begin{aligned}\dot{\mathcal{V}}_2 =& \sum_{i=1}^{N}\mu_i m_i\dot{\beta}_{1i}\dot{x}_i(l_i) + \sum_{i=1}^{N}\mu_i\beta_{1i}\Big[\Gamma_{1i} + v_{1i} + e_{1i} + \mathcal{W}_{1i}^{*\mathrm{T}}\Phi_{1i}(\bar{\mathcal{X}}_{1i}) + \mathcal{D}_{1i}\Big]\\ &+ \sum_{i=1}^{N}\mu_i I_{hi}\dot{\beta}_{2i}\dot{\theta}_i + \sum_{i=1}^{N}\mu_i\beta_{2i}\Big[\Gamma_{2i} + v_{2i} + e_{2i} + \mathcal{W}_{2i}^{*\mathrm{T}}\Phi_{2i}(\bar{\mathcal{X}}_{2i}) + \mathcal{D}_{2i}\Big]\\ &- \lambda_m(\mu T\bar{\mathcal{H}})\sum_{i=1}^{N}\int_0^{l_i}(y_i'(s))^2\mathrm{d}s + \lambda_M(\mu\rho\bar{\mathcal{H}})\sum_{i=1}^{N}\int_0^{l_i}\dot{x}_i^2(s)\mathrm{d}s\\ &- \lambda_m(\mu EI\bar{\mathcal{H}})\int_0^{l_i}(y_i''(s))^2\mathrm{d}s - \sum_{i=1}^{N}\int_0^{l_i}\mu_i c_i x_{ei}(s)\dot{x}_i(s)\mathrm{d}s,\end{aligned} \tag{42}$$

where $\lambda_m(\star)$ denotes the minimum eigenvalue of matrix $\star$.

Moreover, one can calculate the time derivative of $\mathcal{V}_3$ as

$$\begin{aligned}\dot{\mathcal{V}}_3 =&\sum_{i=1}^{N}\sum_{m=1}^{2}\mu_i k_{mi}\beta_{mi}\dot{\beta}_{mi}+\sum_{i=1}^{N}\nu_i\dot{x}_i(l_i)\Big[\Gamma_{1i}+v_{1i}+e_{1i}+\mathcal{W}_{1i}^{*\mathrm{T}}\Phi_{1i}(\bar{\mathcal{X}}_{1i})+\mathcal{D}_{1i}\Big]\\&+\sum_{i=1}^{N}\int_0^{l_i}c_i\mu_i x_{ei}(s)\dot{x}_i(s)\mathrm{d}s+\sum_{i=1}^{N}\nu_i\dot{\theta}_i\Big[\Gamma_{2i}+v_{2i}+e_{2i}+\mathcal{W}_{2i}^{*\mathrm{T}}\Phi_{2i}(\bar{\mathcal{X}}_{2i})+\mathcal{D}_{2i}\Big].\end{aligned}\tag{43}$$

By integrating the above results, we can get

$$\begin{aligned}\dot{\mathcal{V}}_0 =&\sum_{i=1}^{N}\mu_i\Big[k_{1i}\beta_{1i}+m_i\dot{x}_i(l_i)\Big]\dot{\beta}_{1i}+\sum_{i=1}^{N}\sum_{m=1}^{2}s_{mi}\Big[v_{mi}+e_{mi}+\mathcal{W}_{mi}^{*\mathrm{T}}\Phi_{mi}(\bar{\mathcal{X}}_{mi})+\mathcal{D}_{mi}\Big]\\&+\sum_{i=1}^{N}\mu_i\Big[k_{2i}\beta_{2i}+I_{hi}\dot{\theta}_i\Big]\dot{\beta}_{2i}-\Big[\lambda_m(\mu c)-\lambda_M(\mu\rho\bar{\mathcal{H}})\Big]\sum_{i=1}^{N}\int_0^{l_i}\dot{x}_i^2(s)\mathrm{d}s\\&-\lambda_m(\mu T\bar{\mathcal{H}})\sum_{i=1}^{N}\int_0^{l_i}(y_i'(s))^2\mathrm{d}s-\lambda_m(\mu EI\bar{\mathcal{H}})\int_0^{l_i}(y_i''(s))^2\mathrm{d}s,\end{aligned}\tag{44}$$

where $s_{1i}=\mu_i\beta_{1i}+\nu_i\dot{x}_i(l_i)$, $s_{2i}=\mu_i\beta_{2i}+\nu_i\dot{\theta}_i$.

Secondly, to constrain the performances of consensus tracking errors, consider the tangent-type BLF

$$\mathcal{V}_4=\frac{1}{2}\sum_{m=1}^{2}\sum_{i=1}^{N}q(\beta_{mi})\frac{\bar{h}_{mi}^2}{\pi}\tan\left(\frac{\pi\beta_{mi}^2}{2\bar{h}_{mi}^2}\right)+\frac{1}{2}\sum_{m=1}^{2}\sum_{i=1}^{N}(1-q(\beta_{mi}))\frac{\underline{h}_{mi}^2}{\pi}\tan\left(\frac{\pi\beta_{mi}^2}{2\underline{h}_{mi}^2}\right).\tag{45}$$

Taking the time derivative of (45) and using (7), one obtains

$$\dot{\mathcal{V}}_4=\sum_{m=1}^{2}\sum_{i=1}^{N}q(\beta_{mi})\beta_{mi}\sec^2\left(\frac{\pi\beta_{mi}^2}{2\bar{h}_{mi}^2}\right)\dot{\beta}_{mi}+\sum_{m=1}^{2}\sum_{i=1}^{N}(1-q(\beta_{mi}))\beta_{mi}\sec^2\left(\frac{\pi\beta_{mi}^2}{2\underline{h}_{mi}^2}\right)\dot{\beta}_{mi}.\tag{46}$$

Thirdly, choose the following Lyapunov function as:

$$\mathcal{V}_5=\frac{1}{2}\sum_{m=1}^{2}\sum_{i=1}^{N}(\sigma_m^{-1}\tilde{\mathcal{W}}_{mi}^{\mathrm{T}}\tilde{\mathcal{W}}_{mi}+\varpi_m^{-1}\tilde{\bar{\mathcal{D}}}_{mi}^2),\tag{47}$$

where $\tilde{\mathcal{W}}_{mi}=\mathcal{W}_{mi}^*-\hat{\mathcal{W}}_{mi}$ is the estimation error of the unknown ideal weight matrix and $\tilde{\mathcal{D}}_{mi}=\bar{\mathcal{D}}_{mi}-\hat{\mathcal{D}}_{mi}$ is the estimation error of $\bar{\mathcal{D}}_m$, $m=1,2$.

By substituting (27) and (28) and applying Lemma 2, one can estimate $\dot{\mathcal{V}}_5$ as

$$\begin{aligned}\dot{\mathcal{V}}_5\leqslant&-\sum_{m=1}^{2}\sum_{i=1}^{N}\frac{s_{mi}^2\tilde{\mathcal{D}}_{mi}}{|s_{mi}|+\varphi_{mi}}-\sum_{i=1}^{N}\sum_{m=1}^{2}s_{mi}\tilde{\mathcal{W}}_{mi}^{\mathrm{T}}\Phi_{mi}(\bar{\mathcal{X}}_{mi})-\frac{1}{2}\sum_{m=1}^{2}\sum_{i=1}^{N}\varrho_{mi}\|\tilde{\mathcal{W}}_{mi}\|_2^2\\&+\frac{1}{2}\sum_{m=1}^{2}\sum_{i=1}^{N}\varrho_{mi}\|\mathcal{W}_{mi}^*\|_2^2-\frac{1}{2}\sum_{m=1}^{2}\sum_{i=1}^{N}\varrho_{mi}\tilde{\mathcal{D}}_{mi}^2+\frac{1}{2}\sum_{m=1}^{2}\sum_{i=1}^{N}\varrho_{mi}\bar{\mathcal{D}}_{mi}^2.\end{aligned}\tag{48}$$

The term $\frac{s_m\hat{\mathcal{D}}_m}{|s_m|+\varphi_m}$ in (26) is to compensate for unknown disturbances. Actually, it leads to

$$\sum_{m=1}^{2}s_m^{\mathrm{T}}\left(\mathcal{D}_m-\frac{s_m\hat{\mathcal{D}}_m}{|s_m|+\varphi_m}\right)\leqslant\sum_{m=1}^{2}\sum_{i=1}^{N}\left(\frac{s_{mi}^2\tilde{\mathcal{D}}_{mi}}{|s_{mi}|+\varphi_{mi}}+\bar{\mathcal{D}}_{mi}\varphi_{mi}\right).\tag{49}$$

Finally, take the following Lyapunov function as:

$$\mathcal{V}_6=\mathcal{V}_0+\mathcal{V}_4+\mathcal{V}_5+\sum_{m=1}^{2}\sum_{i=1}^{N}g_{mi}.\tag{50}$$

Then, it can obtain

$$\dot{\mathcal{V}}_6 = \dot{\mathcal{V}}_0 + \dot{\mathcal{V}}_4 + \dot{\mathcal{V}}_5 + \sum_{m=1}^{2}\sum_{i=1}^{N}\bar{\delta}_{mi}\gamma_{mi}s_{mi}^2 - \sum_{m=1}^{2}\sum_{i=1}^{N}\bar{\delta}_{mi}e_{mi}^2 + \sum_{m=1}^{2}\sum_{i=1}^{N}\bar{\delta}_{mi}\bar{\varphi}_{mi}. \tag{51}$$

Using Lemma 1 and (44), (46) and (48), (51), and substituting the control design (26), we can get

$$\begin{aligned}\dot{\mathcal{V}}_6 \leqslant & -\left[\lambda_m(\mu c) - \lambda_M(\mu\rho\bar{\mathcal{H}})\right]\sum_{i=1}^{N}\int_0^{l_i}\dot{x}_i^2(s)\mathrm{d}s - \lambda_m(\mu T\bar{\mathcal{H}})\sum_{i=1}^{N}\int_0^{l_i}(y_i'(s))^2\mathrm{d}s \\ & - \lambda_m(\mu EI\bar{\mathcal{H}})\sum_{i=1}^{N}\int_0^{l_i}(y_i''(s))^2\mathrm{d}s - \sum_{m=1}^{2}\sum_{i=1}^{N}\bar{\kappa}_{mi}\beta_{mi}^2 - \sum_{m=1}^{2}\sum_{i=1}^{N}\left(\kappa_{mi} - \bar{\delta}_{mi}\gamma_{mi} - \frac{1}{2}\right)s_{mi}^2 \\ & - \sum_{m=1}^{2}\sum_{i=1}^{N}\left(\bar{\delta}_{mi} - \frac{1}{2}\right)e_{mi}^2 - \lambda_m((\nu k_1 - \mu m)\bar{\mathcal{H}})\sum_{i=1}^{N}\dot{x}_i^2(l_i) - \lambda_m((\nu k_2 - \mu I_h)\bar{\mathcal{H}})\sum_{i=1}^{N}\dot{\theta}_i^2 \\ & - \sum_{m=1}^{2}\beta_m^{\mathrm{T}}q(\beta_m)\sec^2\left(\frac{\pi\beta_m^2}{2\bar{h}_m^2}\right)\nu^{-1}\mu\bar{\mathcal{H}}\beta_m - \sum_{m=1}^{2}\beta_m^{\mathrm{T}}(1-q(\beta_m))\sec^2\left(\frac{\pi\beta_m^2}{2\underline{h}_m^2}\right)\nu^{-1}\mu\bar{\mathcal{H}}\beta_m \\ & + \sum_{m=1}^{2}\sum_{i=1}^{N}(\bar{D}_{mi}\varphi_{mi} + \bar{\delta}_{mi}\bar{\varphi}_{mi}) + \frac{1}{2}\sum_{m=1}^{2}\sum_{i=1}^{N}(\|\mathcal{W}_{mi}^*\|_2^2 + \bar{\mathcal{D}}_{mi}^2)\varrho_{mi}.\end{aligned} \tag{52}$$

If we can take some appropriate parameters such that $\lambda_m(\mu c) - \lambda_M(\mu\rho\bar{\mathcal{H}}) > 0$, $\lambda_m(\nu k_1 - \mu m) \geqslant 0$, $\lambda_m(\nu k_2 - \mu I_h) \geqslant 0$, $\kappa_{mi} - \bar{\delta}_{mi}\gamma_{mi} - \frac{1}{2} \geqslant 0$, $\bar{\delta}_{mi} - \frac{1}{2} \geqslant 0$, then it can further yield

$$\begin{aligned}\dot{\mathcal{V}}_6 \leqslant & -\iota\mathcal{V}_1 - \min\left\{\frac{2\bar{\kappa}_{mi}}{k_{mi}}\right\}\frac{1}{2}\sum_{m=1}^{2}\sum_{i=1}^{N}k_{mi}\mu_i\beta_{mi}^2 \\ & + \sum_{m=1}^{2}\sum_{i=1}^{N}(\bar{D}_{mi}\varphi_{mi} + \bar{\delta}_{mi}\bar{\varphi}_{mi}) + \frac{1}{2}\sum_{m=1}^{2}\sum_{i=1}^{N}(\|\mathcal{W}_{mi}^*\|_2^2 + \bar{\mathcal{D}}_{mi}^2)\varrho_{mi},\end{aligned} \tag{53}$$

where $\iota = \min\{\frac{2(\lambda_m(\mu c)-\lambda_M(\mu\rho\bar{\mathcal{H}}))}{v_i\rho_i}, \frac{2\lambda_m(\mu T\bar{\mathcal{H}})}{v_iT_i}, \frac{\lambda_m(\mu EI\bar{\mathcal{H}})}{v_iE_iI_i}\}$.

3.3 Stability analysis

In the sequel, stability analysis of the closed-loop network under a signed digraph is provided.

Theorem 1. Consider the networked flexible-link manipulator (1a)–(1d) under the boundary consensus control (26) and the dynamic triggering mechanism (29)–(32). If the initial conditions are bounded and Assumption 1 are satisfied, and there exist positive constants $\varsigma_1, \varsigma_2, \varsigma_3$ and some positive definite diagonal matrices μ, ν, K_1, K_2 such that $0 < \Xi < 1$ with $\Xi = \max\{\lambda_M(\varsigma_1 c^{-1}\rho\bar{\mathcal{H}}), \lambda_M(\varsigma_1^{-1}\mu\nu^{-1}), \lambda_M(\varsigma_2 M K_1^{-1}), \lambda_M(\varsigma_2^{-1}\mu\nu^{-1}), \lambda_M(\varsigma_3 I_h K_2^{-1}), \lambda_M(\varsigma_3^{-1}\mu\nu^{-1})\}$, and there are some appropriate parameters $\bar{\delta}_{mi}$ and γ_{mi} such that

$$\lambda_m(\mu c) - \lambda_M(\mu\rho\bar{\mathcal{H}}) > 0,\ \lambda_m(\nu k_1 - \mu m) \geqslant 0, \tag{54}$$

$$\lambda_m(\nu k_2 - \mu I_h) \geqslant 0,\ \kappa_{mi} - \bar{\delta}_{mi}\gamma_{mi} - \frac{1}{2} \geqslant 0,\ \bar{\delta}_{mi} - \frac{1}{2} \geqslant 0, \tag{55}$$

then the following several statements hold.

(1) Each manipulator agent can achieve the bipartite consensus tracking (5), and their velocities are zero, i.e., $\lim_{t\to\infty}|\theta_i - a_i\theta_d| = 0$, $\lim_{t\to\infty}|x_i(l_i) - a_il\theta_d| = 0$ and $\lim_{t\to\infty}\dot{\theta}_i = 0$, $\lim_{t\to\infty}\dot{x}_i(l_i) = 0$ when $a_i = 1$ if $i \in \mathcal{V}_{\mathcal{G}p}$ and $a_i = -1$ if $i \in \mathcal{V}_{\mathcal{G}3-p}$, $p = 1, 2$.

(2) Vibration displacement is convergent to zero, i.e., $\lim_{t\to\infty} y_i(s) = 0$ for $\forall s \in [0, l]$, $i = 1, \ldots, N$.

(3) If the initial condition $\beta_{mi}(0)$ satisfies (8), then tracking errors α_{1i} and α_{2i} are restrained as $(\underline{\varrho}_{mi}, \bar{\varrho}_{mi})$ where $\underline{\varrho}_m = [\underline{\varrho}_{m1}, \ldots, \underline{\varrho}_{mN}]^{\mathrm{T}}$, $\bar{\varrho}_m = [\bar{\varrho}_{m1}, \ldots, \bar{\varrho}_{mN}]^{\mathrm{T}}$ and $\underline{\varrho}_m = \bar{\mathcal{H}}^{-1}\underline{h}_m$, $\bar{\varrho}_m = \bar{\mathcal{H}}^{-1}\bar{h}_m$, $m = 1, 2$.

(4) Each manipulator agent can avoid Zeno behaviors.

Proof. Based on (53), we further have

$$\dot{\mathcal{V}}_6 \leqslant -\bar{\iota}\left(\mathcal{V}_1+\frac{1}{2}\sum_{m=1}^{2}\sum_{i=1}^{N}k_{mi}\mu_i\beta_{mi}^2\right)+\sum_{m=1}^{2}\sum_{i=1}^{N}(\bar{D}_{mi}\varphi_{mi}+\bar{\delta}_{mi}\bar{\varphi}_{mi})+\frac{1}{2}\sum_{m=1}^{2}\sum_{i=1}^{N}(\|\mathcal{W}_{mi}^*\|_2^2+\bar{\mathcal{D}}_{mi}^2)\varrho_{mi}, \quad (56)$$

where $\bar{\iota}=\min\{\iota,\min\{\frac{2\bar{\kappa}_{mi}}{k_{mi}}\}\}$.

From (56) and (58), one obtains that $\mathcal{V}_6\in\mathcal{L}_\infty(0,\infty)$ and thereby $\mathcal{V}_1\in\mathcal{L}_\infty(0,\infty)$, $\beta_{mi}\in\mathcal{L}_\infty(0,\infty)$, $\dot{\beta}_{mi}\in\mathcal{L}_\infty(0,\infty)$. By referring to [14], it can follow from $\mathcal{V}_1\in\mathcal{L}_\infty(0,\infty)$ that $\Gamma_{1i}\in\mathcal{L}_\infty(0,\infty)$ and $\Gamma_{2i}\in\mathcal{L}_\infty(0,\infty)$. Based on (41), we can know that $\dot{\mathcal{V}}_1+\sum_{m=1}^{2}\sum_{i=1}^{N}k_{mi}\mu_i\beta_{mi}\dot{\beta}_{mi}$ is bounded. Since $\mathcal{V}_1+\frac{1}{2}\sum_{m=1}^{2}\sum_{i=1}^{N}k_{mi}\mu_i\beta_{mi}^2\leqslant\mathcal{V}_6$ and $0\leqslant\varphi_{mi}\in\mathcal{L}_1(0,\infty)$, $0\leqslant\bar{\varphi}_{mi}\in\mathcal{L}_1(0,\infty)$, $0\leqslant\varrho_{mi}\in\mathcal{L}_1(0,\infty)$, it can follow from the proposed Lemma 4 that $\mathcal{V}_1\to 0$ and $\sum_{m=1}^{2}\sum_{i=1}^{N}\beta_{mi}^2\to 0$ when $t\to\infty$. This implies $\alpha_{mi}\to 0$ when $t\to\infty$ and thereby the asymptotical bipartite consensus tracking (5) can be achieved.

On the other hand, using Lemma 2, we have

$$\frac{y_i^2(s)}{2l_i\lambda_{\min}(\nu T)}\leqslant\frac{1}{2}\sum_{i=1}^{N}\int_0^{l_i}\nu_i T_i(y_i'(s))^2\mathrm{d}s\leqslant\mathcal{V}_1, \quad (57)$$

which implies that $y_i(s)\to 0$ when $t\to\infty$. As a result, the statement (2) holds.

By integrating left and right of (56) from 0 to t and $\mathcal{V}_1$ is non-negative, it results in

$$\mathcal{V}_6\leqslant\mathcal{V}_6(0)+\sum_{m=1}^{2}\sum_{i=1}^{N}\left[\bar{D}_{mi}\|\varphi_{mi}\|_{\mathcal{L}_1(0,\infty)}+\bar{\delta}_{mi}\|\bar{\varphi}_{mi}\|_{\mathcal{L}_1(0,\infty)}+(\|\mathcal{W}_{mi}^*\|_2^2+\bar{\mathcal{D}}_{mi}^2)\|\varrho_{mi}\|_{\mathcal{L}_1(0,\infty)}\right]<\infty, \quad (58)$$

which indicates that $\mathcal{V}_6$ is bounded and thereby $\mathcal{V}_4$ is also bounded. Then, we can draw a conclusion that the output constraint (8) is always satisfied according to the boundedness of $\mathcal{V}_4$. It implies $-\underline{h}_m<\bar{\mathcal{H}}\alpha_m<\bar{h}_m$. Furthermore, we can obtain $-\bar{\mathcal{H}}^{-1}\underline{h}_m<\alpha_m<\bar{\mathcal{H}}^{-1}\bar{h}_m$, which ensures the transient performances of the tracking error α_{mi}. Hence, the statement (3) is proved.

Since $g_{mi}\geqslant g_{mi}(0)\mathrm{e}^{-\bar{\delta}_{mi}t}\geqslant g_{mi}(0)\mathrm{e}^{-(\varepsilon_{mi}+\bar{\delta}_{mi})t}$, the dwell time between two consecutive triggering instants is bigger than the dynamic triggered mechanisms in [39,42], where the interval internal variable is $\dot{g}_{mi}=-\varepsilon_{mi}g_{mi}+\bar{\delta}_{mi}(\gamma_{mi}s_{mi}^2-e_{mi}^2)$. The dynamic triggered mechanisms in [39,42] have been proven that the minimum dwell time is strictly greater than zero. Hence, Zeno behaviors can excluded for each manipulator agent for our proposed dynamic triggered mechanism, i.e., the statement (4) is satisfied.

4 Numerical simulations

To illustrate the feasibility of the proposed control algorithm, a numerical example is provided. As shown in Figure 3, consider a signed graph including six agents labeled by 0 to 6. Obviously, Assumption 1 is satisfied. By using the signed graph theory, one can obtain $\bar{\mathcal{H}}$. In the agent network, all follower agents from 1 to 6 are taken as flexible manipulators described by (1a)–(1d). The corresponding system parameters are set as $l=1.0$ m, $E_iI_i=2.0+0.01i$ N·m^2, $T=10.0+0.02i$ N, $I_{hi}=0.10+0.01i$ kg·m^2, $m_i=2.5+0.1i$ kg, $\rho_i=0.1+0.01i$ kg/m, $c_i=20$ N·s/m. Moreover, the time-varying disturbances are taken as $d_{1i}=0.1i+\sin(it)+\sin(0.5it)$ and $d_{2i}=0.1i+\cos(t)+\cos(0.5t)$, and modeling uncertainty functions $f_{1i}=0.2\sin(x_i(l_i))\dot{x}_i(l_i)+0.1y_i'''(l_i)$, $f_{2i}=0.1i\sin(\theta_i\dot{\theta}_i)+0.2y_i''(0)$. The initial conditions $y_i(s,0)=\dot{y}_i(s,0)=\theta_i(0)=\dot{\theta}_i(0)=0$, where $i=1,\ldots,6$. Agent 0 is the reference angle signal with $\theta_d=0.5$ rad. Considering boundary control inputs are affected by saturations and backlashes, let $p_{1i}=0.6$, $p_{2i}=0.5$, $B_{r1i}=0.2$, $B_{l1i}=-0.1$, $B_{r2i}=0.2$, $B_{l2i}=-0.1$, $u_{Lmi}=-10$, $u_{Rmi}=10$, where $i=1,\ldots,6$, $m=1,2$. By using the finite difference method [13], the numerical simulations are given.

Case 1. Without boundary control inputs, i.e., $u_{mi}=0$ for any $m=1,2$, and $i=1,\ldots,6$. The corresponding system responses are shown in Figures 4–6, when no boundary driving forces are applied to these manipulator agents. As shown in Figures 4 and 5, due to the influence of external disturbances and modeling uncertainties, the top displacement $x_i(l_i)$ and the steering angle θ_i of the manipulator agent cannot track the desired signal, where $i=1,\ldots,6$. Hence, it is impossible to use these manipulators to complete the established work goals. Moreover, it can be seen from Figure 6 that the vibration displacement $y_i(s)$ fluctuates with time, which affects the work efficiency of manipulators, where $i=1,\ldots,6$. To enable all manipulators to work, the controlled case is provided.

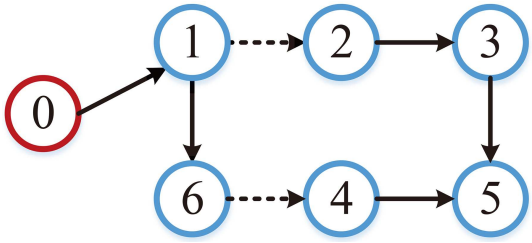

Figure 3 (Color online) Signed diagraph $\bar{\mathcal{G}}$ where the solid (dashed) lines denote the cooperative (antagonistic) interactions.

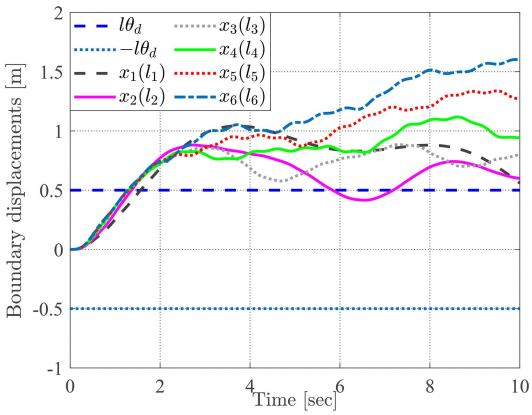

Figure 4 (Color online) Boundary displacement $x_i(l_i)$ of manipulator agent without control, where $i = 1, \ldots, 6$.

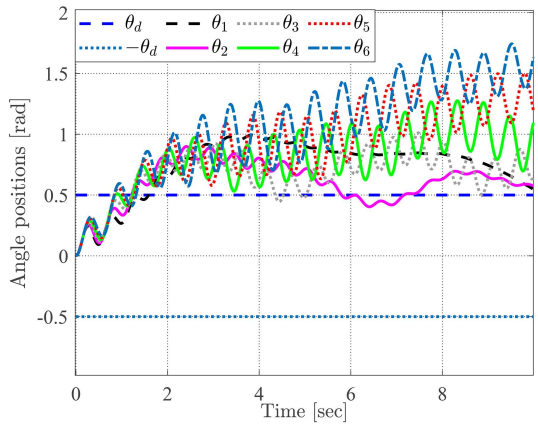

Figure 5 (Color online) Angle position θ_i of manipulator agent without control, where $i = 1, \ldots, 6$.

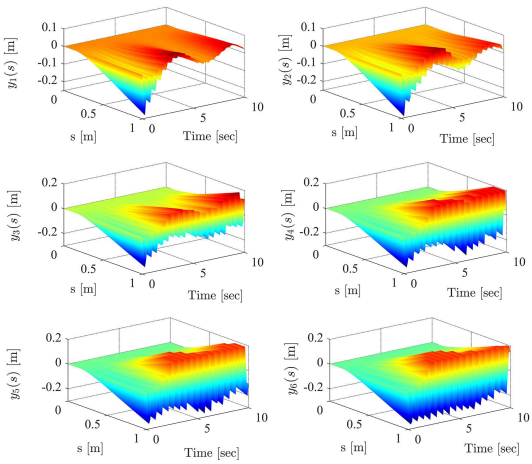

Figure 6 (Color online) Vibration displacement $y_i(s)$ of manipulator agent without control, where $s \in [0, l]$ and $i = 1, \ldots, 6$.

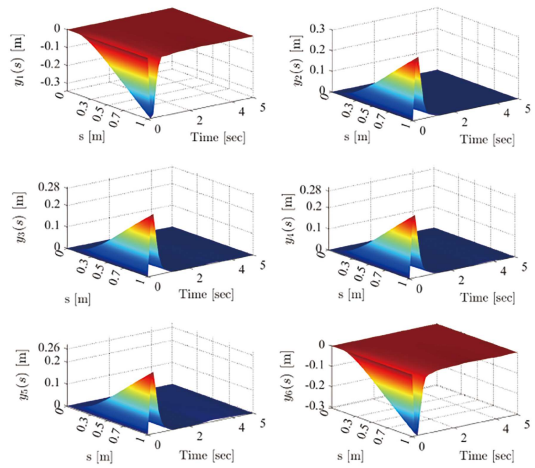

Figure 7 (Color online) Vibration displacement $y_i(s)$ of manipulator agent with event-based control, where $s \in [0, l]$ and $i = 1, \ldots, 6$.

Case 2. Under the proposed event-based control inputs described by (26) and (29)–(32). The corresponding control parameters are taken as $k_1 = \text{diag}\{25, 100, 100, 100, 100, 100\}$, $k_2 = \text{diag}\{2, 4, 4, 4, 4, 4\}$, and $\kappa_1 = \text{diag}\{7.5, 30, 30, 30, 30, 30\}$, $\kappa_2 = \text{diag}\{5, 10, 10, 10, 10, 10\}$, and $\bar{\kappa}_1 = 30I_6$, $\bar{\kappa}_2 = 5I_6$, $\mu = \text{diag}\{10, 20, 20, 20, 20, 20\}$, $\nu = 2I_6$. Moreover, adaptive parameters are chosen as $\sigma_1 = 1I_6$, $\sigma_2 = 2I_6$, $\varpi_1 = 5I_6$, $\varpi_2 = 0.1I_6$ and $\varrho_{mi} = \varphi_{mi} = \mathrm{e}^{-t}$ for $i = 1, \ldots, 6$ and $m = 1, 2$. In the dynamic event-triggering mechanism (29)–(32), let $\gamma_1 = 5I_6$, $\bar{\delta}_1 = 2I_6$, $\gamma_2 = 0.8I_6$, $\bar{\delta}_2 = 1I_6$, and $g_1(0) = 1.5I_6$, $g_2(0) = 0.5I_6$, $\bar{\varphi}_{mi} = 2\mathrm{e}^{-0.5t}$, where $i = 1, \ldots, 6$ and $m = 1, 2$. The output constraint boundary coefficients are considered as $\underline{h}_1 = -25I_6$, $\bar{h}_1 = 25I_6$, $\underline{h}_2 = -26I_6$, $\bar{h}_2 = 26I_6$. By taking $\varsigma_{1i} = \varsigma_{2i} = \varsigma_{3i} = 12.5$, $\bar{\delta}_{1i} = 5$, $\bar{\delta}_{2i} = 1.5$, $\gamma_{1i} = 1$, $\gamma_{2i} = 0.6$, we can obtain that $\kappa = 0.9762$, $\lambda_m(\mu c) - \lambda_M(\mu\rho\bar{\mathcal{H}}) = 18.7550$, $\lambda_m(\nu k_1 - \mu m) = 24$,

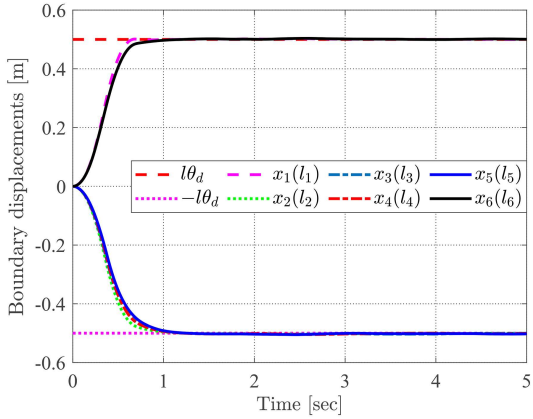

Figure 8 (Color online) Boundary displacement $x_i(l_i)$ of manipulator agent with event-based control, where $i = 1, \ldots, 6$.

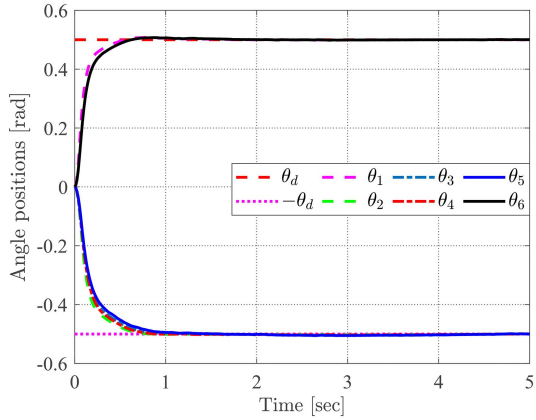

Figure 9 (Color online) Angle position θ_i of manipulator agent with event-based control, where $i = 1, \ldots, 6$.

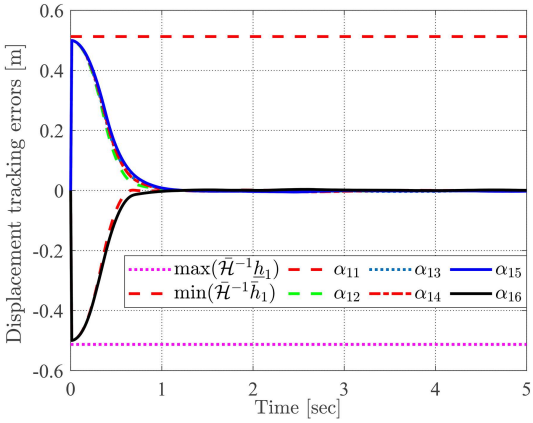

Figure 10 (Color online) Constraint control of α_{1i} with event-based control, where $i = 1, \ldots, 6$.

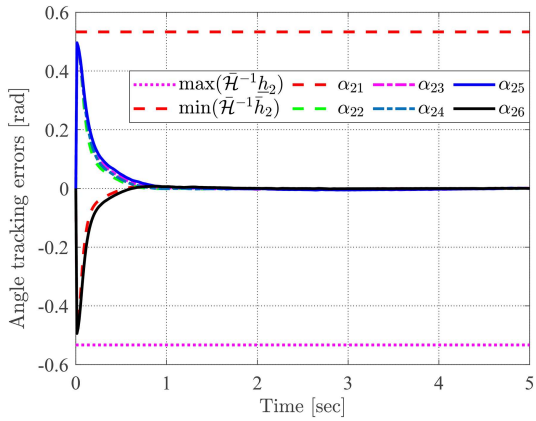

Figure 11 (Color online) Constraint control of α_{2i} with event-based control, where $i = 1, \ldots, 6$.

$\lambda_m(\nu k_2 - \mu I_h) = 2.8$, $\min\{\kappa_{mi} - \bar{\delta}_{mi}\gamma_{mi} - \frac{1}{2}\} = \min\{4.5, 3.7\} = 3.7$, $\min\{\bar{\delta}_{mi} - \frac{1}{2}\} = \min\{1.5, 0.5\} = 0.5$. Therefore, $0 < \Xi < 1$ and inequalities (54) and (55) are all satisfied in Theorem 1. Based on these control parameters and using the designed boundary control strategy, the controlled systems' responses are provided in Figures 7–9. From Figure 7, vibration displacement $y_i(s)$ of the manipulator agent is quickly and well suppressed under the designed boundary event-based control inputs, where $i = 1, \ldots, 6$. Besides, from Figures 8 and 9, it can be found that these manipulator agents quickly achieve the bipartite consensus tracking (5) before two seconds, even manipulator systems have multiple constraints such as time-varying disturbances and modeling uncertainties, unknown input saturations and backlashes. Moreover, the output constraints of tracking errors are shown in Figures 10 and 11. From Figures 10 and 11, we can observe that the output constraints of tracking errors can be satisfied with the proposed boundary event-based control laws. In summary, numerical simulations illustrate the effectiveness of the proposed boundary event-based consensus control strategy, which has a great significance to ensure that manipulators work together and improve work efficiency.

On the other hand, the event triggering numbers of all manipulators with two different boundary control inputs are 112, 209, 138, 132, 110, 183, and 200, 216, 159, 161, 135, 195. The second control input has a greater number of triggers than the first. For the first control input, the maximum event-triggering rate of the flexible manipulator agent is $\frac{209}{20000} = 1.045\%$. The maximum event-triggering rate for the second control input is $\frac{216}{20000} = 1.08\%$. This demonstrates that using the proposed event-based law, two control inputs of all manipulators can avoid a large number of updates, thereby conserving control resources. Applying event-based control design is based on the fundamental idea of avoiding Zeno behaviors. To show that the suggested control algorithm is capable of avoiding Zeno behaviors, Figures 12 and 13 are given to show the triggering time intervals for two different control inputs of each

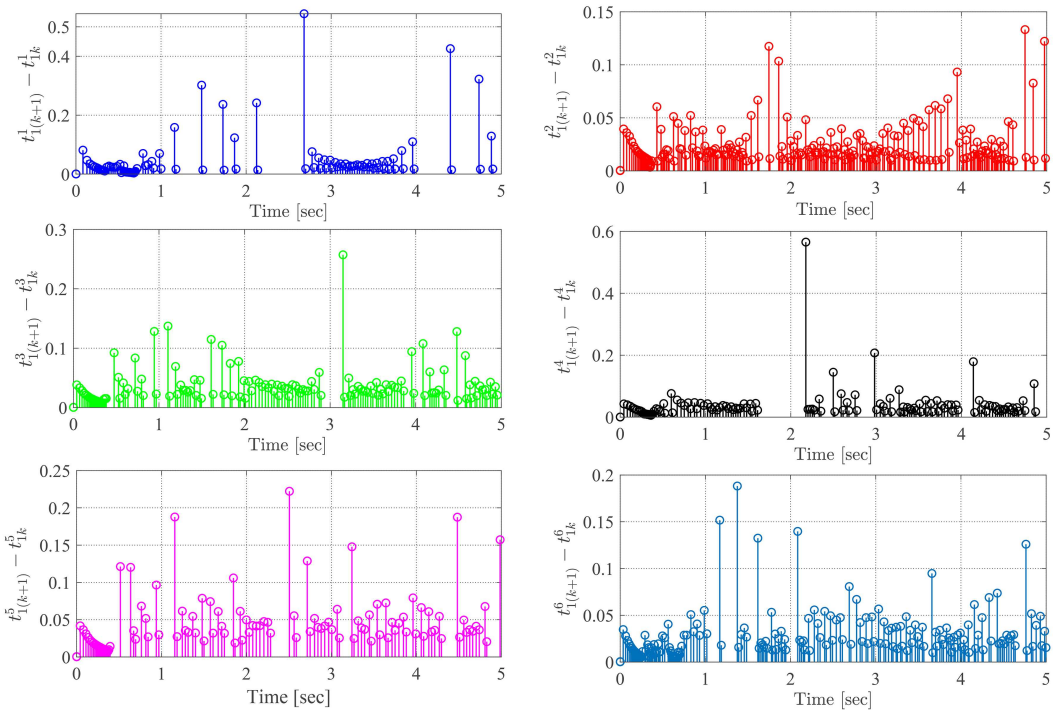

Figure 12 (Color online) Triggering time intervals of the first input.

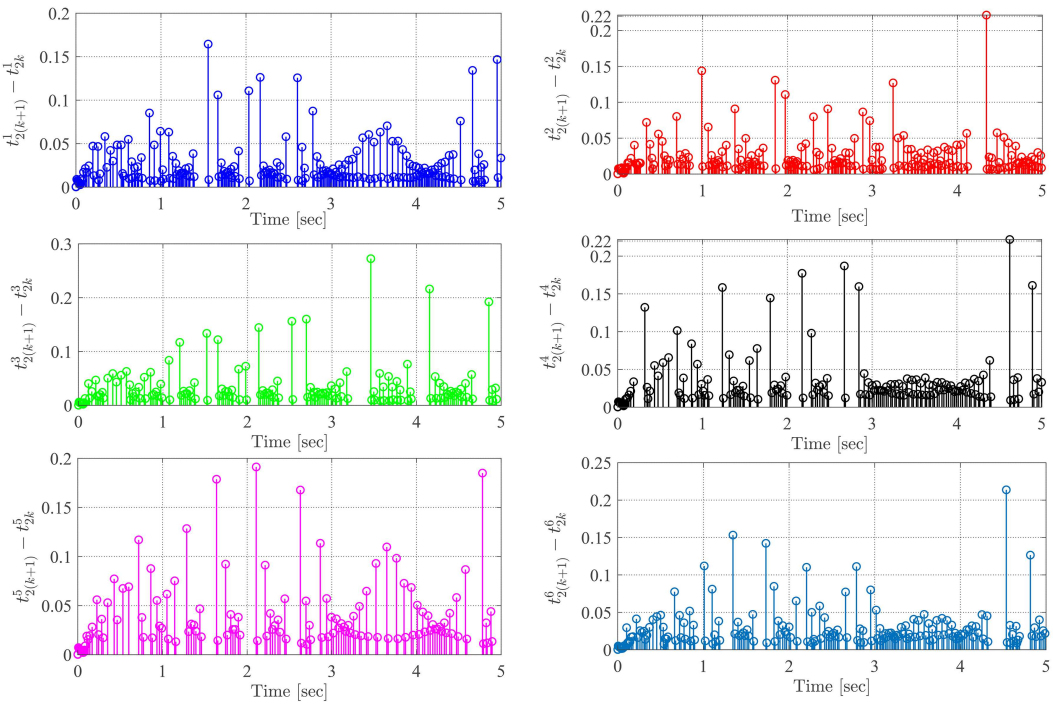

Figure 13 (Color online) Triggering time intervals of the second input.

manipulator agent. From Figures 12 and 13, their event-based dwell-times are strictly bigger than zero, implying that all manipulator agents are capable of avoiding Zeno behaviors. As a result, the suggested distributed boundary dynamic ETC is both effective and practical. Ultimately, Figures 14 and 15 offer two distributed boundary control inputs for each manipulator agent. For the first control input, Figure 14 respectively describes three different control inputs including time-triggered control inputs, event-based control inputs, and actual control inputs. Figure 15 respectively shows three different control inputs including time-triggered control inputs, event-based control inputs, and actual control inputs, for

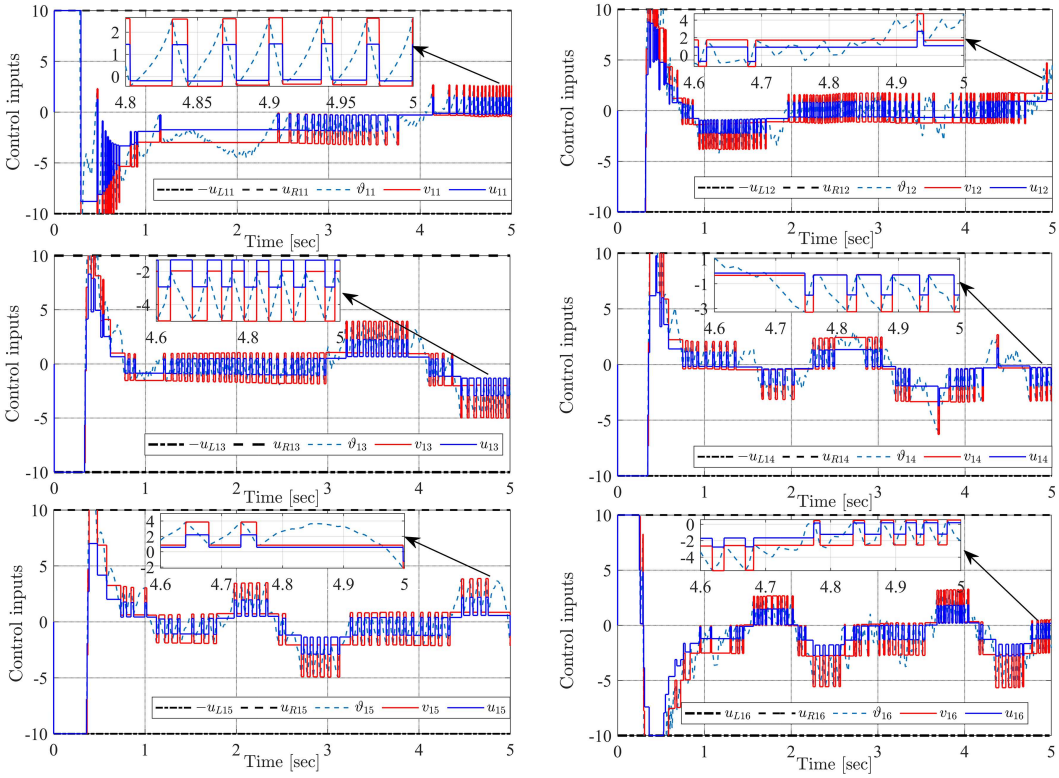

Figure 14 (Color online) The first distributed boundary control inputs.

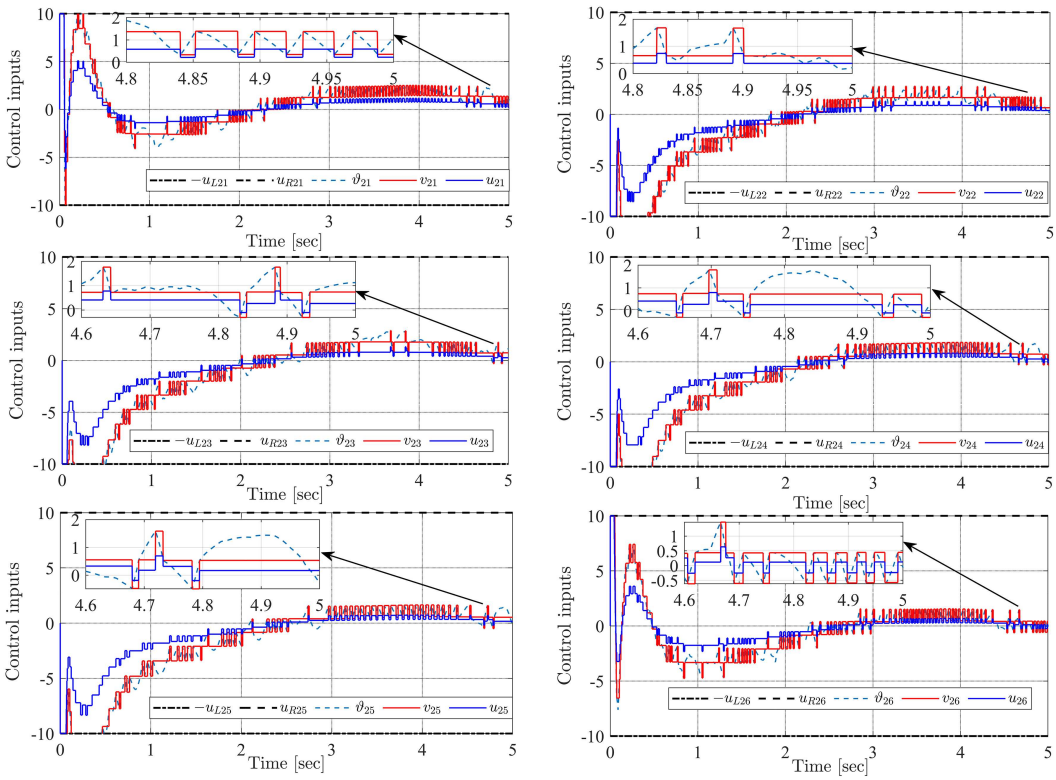

Figure 15 (Color online) The second distributed boundary control inputs.

the second control inputs. As can be seen, event-based control inputs can avoid superfluous controller updates, but actual controllers will decay and shift and have some limited maximum controls under the

Table 1 Event numbers of agent 1.

Method	The first input	The second input	The maximum event-triggering rate (%)
ETC used in [39]	217	287	1.435
ETC used in [43]	143	271	1.355
ETC in this work	112	200	1.00

influence of input saturations and backlashes. In general, we can deduce from the above numerical results that the suggested event-based boundary consensus control algorithm is effective.

To demonstrate the superiority of the proposed approach, we compare them to some existing event-based control strategies proposed in [39, 43]. In [39], the dynamic ETC is chosen as $f_{mi}(e_{mi}, \vartheta_{mi}, t) = \pi_{mi}(|e_{mi}| - \omega_{mi}|\vartheta_{mi}|) - n_{mi}$, and n_{mi} is the interval dynamic variable given by $\dot{n}_{mi} = -\bar{\pi}_{mi}n_{mi} + \bar{\varepsilon}_{mi}(\omega_{mi}|\vartheta_{mi}| - |e_{mi}|)$, where π_{mi}, ω_{mi}, $\bar{\pi}_{mi}$, $\bar{\varepsilon}_{mi}$, are some positive constants. In [43], the triggering function is chosen as $f_{mi}(e_{mi}, s_{mi}, t) = e_{mi}^2 - o_{mi}s_{mi}^2 - \varepsilon_{mi}\mathrm{e}^{-\epsilon_{mi}t}$, where o_{mi}, ε_{mi}, ϵ_{mi}, are some positive constants. By taking $\pi_1 = \bar{\pi}_2 = 20I_6$, $\omega_1 = \bar{\varepsilon}_2 = 0.2I_6$, $n_1(0) = 1.5I_6$, $\pi_2 = \bar{\pi}_2 = 20I_6$, $\omega_2 = \bar{\varepsilon}_2 = 0.3I_6$, $n_2(0) = 0.5I_6$ and $o_1 = \varepsilon_1 = 5I_6$, $\epsilon_1 = 0.5I_6$, $o_2 = 0.8I_6$, $\varepsilon_1 = 0.8I_6$, $\epsilon_2 = 0.5I_6$, the counts of triggers for two boundary different controllers of agent 1 are reported in Table 1. As illustrated in Table 1, the proposed ETC control strategy exhibits the fewest trigger numbers on both the first and second boundary control inputs, thereby demonstrating its superiority over existing methodologies.

5 Conclusion

In this article, we mainly focus on boundary event-based bipartite consensus tracking control of multiple flexible manipulator systems with time-varying disturbances, modeling uncertainties, input saturations and backlashes, and output constraints. In this case, it is a challenging task to achieve the spatial point-by-point asymptotic stabilization of a flexible manipulator. To solve this puzzle, we develop a lemma to build an interesting asymptotically convergent result. By integrating boundary consensus design, BLF, neural network estimation, and dynamic event-triggering method, a new boundary bipartite consensus tracking control algorithm is presented. Under the designed control algorithm and the newly developed lemma, asymptotical bipartite cooperative tracking of multiple manipulators can be realized while suppressing their unfavorable vibration displacements. Finally, simulation results well illustrate the effectiveness of the proposed results.

Acknowledgements This work was supported in part by Key Program of National Natural Science Foundation of China (Grant No. 62433011) and Guangdong Basic and Applied Basic Research Foundation (Grant No. 2021B1515120017).

References

1 Fax J A, Murray R M. Information flow and cooperative control of vehicle formations. IEEE Trans Automat Contr, 2004, 49: 1465–1476
2 Rasmussen S, Schumacher C. Cooperative control of unmanned aerial vehicles. Intl J Robust Nonlinear, 2008, 18: 115–117
3 Jin J, Ma X. A multi-objective agent-based control approach with application in intelligent traffic signal system. IEEE Trans Intell Transp Syst, 2019, 20: 3900–3912
4 Li Z, Wen G, Duan Z, et al. Designing fully distributed consensus protocols for linear multi-agent systems with directed graphs. IEEE Trans Automat Contr, 2015, 60: 1152–1157
5 Altafini C. Consensus problems on networks with antagonistic interactions. IEEE Trans Automat Contr, 2013, 58: 935–946
6 Ning B, Han Q L, Zuo Z. Bipartite consensus tracking for second-order multiagent systems: a time-varying function-based preset-time approach. IEEE Trans Automat Contr, 2020, 66: 2739–2745
7 Li W, Zhang H, Mu Y, et al. Bipartite time-varying output formation tracking for multiagent systems with multiple heterogeneous leaders under signed digraph. IEEE Trans Ind Inf, 2023, 19: 11070–11079
8 Lui D G, Petrillo A, Santini S. Bipartite tracking consensus for high-order heterogeneous uncertain nonlinear multi-agent systems with unknown leader dynamics via adaptive fully-distributed PID control. IEEE Trans Netw Sci Eng, 2023, 10: 1131–1142
9 Lui D G, Petrillo A, Santini S. Exponential bipartite tracking consensus in cooperative-antagonistic nonlinear multi-agent systems with multiple communication time-varying delays. IFAC J Syst Control, 2022, 22: 100209
10 Krstic M, Smyshlyaev A. Boundary Control of PDEs: A Course on Backstepping Designs. Philadelphia: Society for Industrial and Applied Mathematics, 2008
11 Liu Z, Liu J, He W. Robust adaptive fault tolerant control for a linear cascaded ODE-beam system. Automatica, 2018, 98: 42–50
12 He W, He X, Zou M, et al. PDE model-based boundary control design for a flexible robotic manipulator with input backlash. IEEE Trans Contr Syst Technol, 2019, 27: 790–797
13 Liu Y, Chen X, Wu Y, et al. Adaptive neural network control of a flexible spacecraft subject to input nonlinearity and asymmetric output constraint. IEEE Trans Neural Netw Learn Syst, 2022, 33: 6226–6234
14 Liu Z J, Han Z J, Zhao Z J, et al. Modeling and adaptive control for a spatial flexible spacecraft with unknown actuator failures. Sci China Inf Sci, 2021, 64: 152208
15 Zhao Z, Liu Z, He W, et al. Boundary adaptive fault-tolerant control for a flexible Timoshenko arm with backlash-like hysteresis. Automatica, 2021, 130: 109690

16 Liu Y, Liu F, Mei Y, et al. Adaptive neural network vibration control for an output-tension-constrained axially moving belt system with input nonlinearity. IEEE ASME Trans Mechatron, 2021, 27: 656–665
17 Pilloni A, Pisano A, Orlov Y, et al. Consensus-based control for a network of diffusion PDEs with boundary local interaction. IEEE Trans Automat Contr, 2016, 61: 2708–2713
18 Deutscher J. Robust cooperative output regulation for a network of parabolic PDE systems. IEEE Trans Automat Contr, 2022, 67: 451–459
19 Chen Y, Zuo Z, Wang Y. Bipartite consensus for a network of wave PDEs over a signed directed graph. Automatica, 2021, 129: 109640
20 Zheng S, Shi P, Wang S, et al. Adaptive neural control for a class of nonlinear multiagent systems. IEEE Trans Neural Netw Learn Syst, 2021, 32: 763–776
21 Yao X, Zhao W, Liu Y. Adaptive fuzzy-based fault-tolerant boundary control of flexible Timoshenko manipulators under directed graph. IEEE Trans Fuzzy Syst, 2024, 32: 294–305
22 Chen T, Wen H, Wei Z. Distributed attitude tracking for multiple flexible spacecraft described by partial differential equations. Acta Astronaut, 2019, 159: 637–645
23 Han F, Jia Y. Bipartite consensus and distributed boundary control for multiple flexible manipulators associated with signed digraph. IEEE Trans Syst Man Cybern Syst, 2022, 52: 3005–3014
24 Li L, Liu J. Consensus tracking control and vibration suppression for nonlinear mobile flexible manipulator multi-agent systems based on PDE model. Nonlinear Dyn, 2023, 111: 3345–3359
25 Liu Y, Yao X, Zhao W. Distributed neural-based fault-tolerant control of multiple flexible manipulators with input saturations. Automatica, 2023, 156: 111202
26 Zhao W, Liu Y, Yao X. PDE-based boundary adaptive consensus control of multiagent systems with input constraints. IEEE Trans Neural Netw Learn Syst, 2024, 35: 12617–12626
27 Tee K P, Ge S S, Tay E H. Barrier Lyapunov functions for the control of output-constrained nonlinear systems. Automatica, 2009, 45: 918–927
28 Romdlony M Z, Jayawardhana B. Stabilization with guaranteed safety using control Lyapunov-barrier function. Automatica, 2016, 66: 39–47
29 Liu L, Liu Y J, Chen A Q, et al. Integral barrier Lyapunov function-based adaptive control for switched nonlinear systems. Sci China Inf Sci, 2020, 63: 132203
30 Li H, Liu C L, Zhang Y, et al. Practical fixed-time consensus tracking for multiple Euler-Lagrange systems with stochastic packet losses and input/output constraints. IEEE Syst J, 2022, 16: 6185–6196
31 Zhu C, Jiang Y, Yang C. Fixed-time neural control of robot manipulator with global stability and guaranteed transient performance. IEEE Trans Ind Electron, 2023, 70: 803–812
32 Liu Y, Mei Y, Cai H, et al. Asymmetric input-output constraint control of a flexible variable-length rotary crane arm. IEEE Trans Cybern, 2021, 52: 10582–10591
33 Liu Z, Han Z, He W. Adaptive fault-tolerant boundary control of an autonomous aerial refueling hose system with prescribed constraints. IEEE Trans Automat Sci Eng, 2021, 19: 2678–2688
34 Zhao Z, Liu Y, Zou T, et al. Robust adaptive fault-tolerant control for a riser-vessel system with input hysteresis and time-varying output constraints. IEEE Trans Cybern, 2023, 53: 3939–3950
35 Liu Y, Chen X B, Mei Y F, et al. Observer-based boundary control for an asymmetric output-constrained flexible robotic manipulator. Sci China Inf Sci, 2022, 65: 139203
36 Girard A. Dynamic triggering mechanisms for event-triggered control. IEEE Trans Automat Contr, 2014, 60: 1992–1997
37 Chen Z Y, Han Q L, Yan Y M, et al. How often should one update control and estimation: review of networked triggering techniques. Sci China Inf Sci, 2020, 63: 150201
38 Nowzari C, Garcia E, Cortés J. Event-triggered communication and control of networked systems for multi-agent consensus. Automatica, 2019, 105: 1–27
39 Liu Z, Shi J, He Y, et al. Adaptive fuzzy control for a spatial flexible hose system with dynamic event-triggered mechanism. IEEE Trans Aerosp Electron Syst, 2023, 59: 1156–1167
40 Espitia N, Karafyllis I, Krstic M. Event-triggered boundary control of constant-parameter reaction-diffusion PDEs: a small-gain approach. Automatica, 2021, 128: 109562
41 Rathnayake B, Diagne M, Espitia N, et al. Observer-based event-triggered boundary control of a class of reaction-diffusion PDEs. IEEE Trans Automat Contr, 2022, 67: 2905–2917
42 Cao R, Cheng L. Distributed dynamic event-triggered control for Euler-Lagrange multiagent systems with parametric uncertainties. IEEE Trans Cybern, 2023, 53: 1272–1284
43 Cai Y, Zhang H, Li W, et al. Distributed bipartite adaptive event-triggered fault-tolerant consensus tracking for linear multiagent systems under actuator faults. IEEE Trans Cybern, 2022, 52: 11313–11324
44 Li W H, Zhang H G, Zhang J, et al. Fully distributed dynamic event-triggered formation-containment tracking for multiagent systems with multiple types of disturbances. Sci China Inf Sci, 2024, 67: 112203
45 Ioannou P A, Fidan B. Adaptive Control Tutorial. Philadelphia: Society for Industrial and Applied Mathematics, 2006